THE GEOLOGICAL SOCIETY OF AMERICA®

Revised age constraints for Late Cretaceous to early Paleocene terrestrial strata from the Dawson Creek section, Big Bend National Park, west Texas

Caitlin E. Leslie[1,†], Daniel J. Peppe[1], Thomas E. Williamson[2], Matthew Heizler[3], Mike Jackson[4], Stacy C. Atchley[1], Lee Nordt[1], and Barbara Standhardt[5]

[1]*Terrestrial Paleoclimatology Research Group, Department of Geosciences, Baylor University, One Bear Place #97354, Waco, Texas 76706, USA*

[2]*New Mexico Museum of Natural History and Science, Albuquerque, New Mexico 87104, USA*

[3]*New Mexico Bureau of Geology, New Mexico Tech, Socorro, New Mexico 87801, USA*

[4]*Institute for Rock Magnetism, University of Minnesota, Minneapolis, Minnesota 55455, USA*

[5]*14700 FM 307, Stanton, Texas 79782, USA*

ABSTRACT

We analyzed samples for paleomagnetism, $^{40}Ar/^{39}Ar$ detrital sanidine ages, and mammalian fauna to produce a precise chronostratigraphic framework for the Upper Cretaceous to Lower Paleocene Dawson Creek section of Big Bend National Park, west Texas. Prior to this work, the absolute ages and durations of the Upper Cretaceous Aguja and Javelina Formations and Paleocene Black Peaks Formation were relatively poorly constrained. The documented polarity zones can be correlated to C32n-C31n, C29r, and C27r of the geomagnetic polarity time scale, with three hiatuses spanning more than 1.5 m.y. each. Rock magnetic analyses indicate that the dominant magnetic carrier in the Aguja and Black Peaks Formations is titanomagnetite, while the Javelina Formation has varying magnetic carriers, including hematite, magnetite, and maghemite. An overprint interval surrounding the Cretaceous-Paleogene boundary suggests the primary magnetic carrier, titanohematite, was likely reset by burial and/or overlying basaltic flows. These are the first independent age constraints for the Cretaceous–Paleocene strata at the Dawson Creek section that determine the age and duration of deposition of each formation in the section, as well as the age and duration of multiple unconformities through the succession. As a result, these age constraints can be used to reassess biostratigraphic and isotopic correlations between the Big Bend area and other Cretaceous–Paleogene basins across North America. Based on this new data set, we reassign the age of the mammalian fauna found in the Black Peaks Formation from the Puercan to the Torrejonian North American Land Mammal age. Our age constraints show that the dinosaur fauna in the Javelina Formation in the Dawson Creek area is latest Maastrichtian and restricted to chron C29r. Thus, the Javelina dinosaur fauna is correlative to the Hell Creek Formation dinosaur fauna from the Northern Great Plains, indicating differences between the faunas are not due to differences in age, and providing support for the hypothesis of provinciality and endemism in dinosaur communities in the late Maastrichtian. Further, the age constraints indicate that the previously documented mid-Maastrichtian and late Maastrichtian greenhouse events were rapid (<200 k.y.) and correlate closely with climate events documented in the marine record.

INTRODUCTION

The Dawson Creek section within Big Bend National Park, Texas, documents a series of Cretaceous though Lower Paleocene alluvial deposits that accumulated along a passive continental margin within the Tornillo Basin of west Texas (Fig. 1). This coastal plain succession has been the focus of several lithostratigraphic, cyclostratigraphic, paleopedologic, magnetostratigraphic, and paleontologic studies (e.g., Lawson, 1972; Standhardt, 1986; Lehman, 1989a, 1990; Nordt et al., 2003; Atchley et al., 2004). The Cretaceous dinosaur and early Paleocene mammalian faunas from Big Bend, and particularly from the Dawson Creek area, are key elements for understanding regional patterns in dinosaur and mammal community diversity and biostratigraphy. Dawson Creek is the southernmost latest Cretaceous (late Maastrichtian) terrestrial vertebrate fossil site in North America. Therefore, it forms a critical data set that is necessary for assessing patterns of endemism in Campanian and Maastrichtian dinosaur faunas across North America (e.g., Standhardt, 1986; Lehman, 1997, 2001; Lofgren et al., 2004; Sampson et al., 2010; Lucas et al., 2016). Additionally, analyses of paleosols at the Dawson Creek section have been interpreted to indicate two short-lived greenhouse events during the Maastrichtian (Nordt et al., 2003; Dworkin et al., 2005). Despite the importance of the Dawson Creek record for understanding Cretaceous and Paleocene paleoclimate and the composition of vertebrate communities, the absolute ages and durations of the Upper Cretaceous Aguja and Javelina Formations and Paleocene Black Peaks Formation are relatively poorly constrained.

In this study, we developed a precise chronostratigraphic framework for the Dawson Creek section using magnetostratigraphy, $^{40}Ar/^{39}Ar$ detrital sanidine geochronology, and biostratigraphy based on a reevaluation of the vertebrate fauna. From these analyses, we determined the age and duration of deposition for each formation in the section, as well as the age and duration of multiple unconformities through the succession. Finally, we used these new age constraints to assess the implications for biostratigraphic and isotopic correlations between the Big Bend area and other Cretaceous–Paleogene basins across North America and the global marine record.

PREVIOUS WORK

Geochronology

Previous studies used a combination of biostratigraphy, estimates of sedimentation rates based on paleosol maturity, and correlations

†caitlin_leslie@baylor.edu, caitlineleslie@baylor.edu.

GSA Bulletin; https://doi.org/10.1130/B31785.1; 10 figures; 3 tables; Data Repository item 2018042.

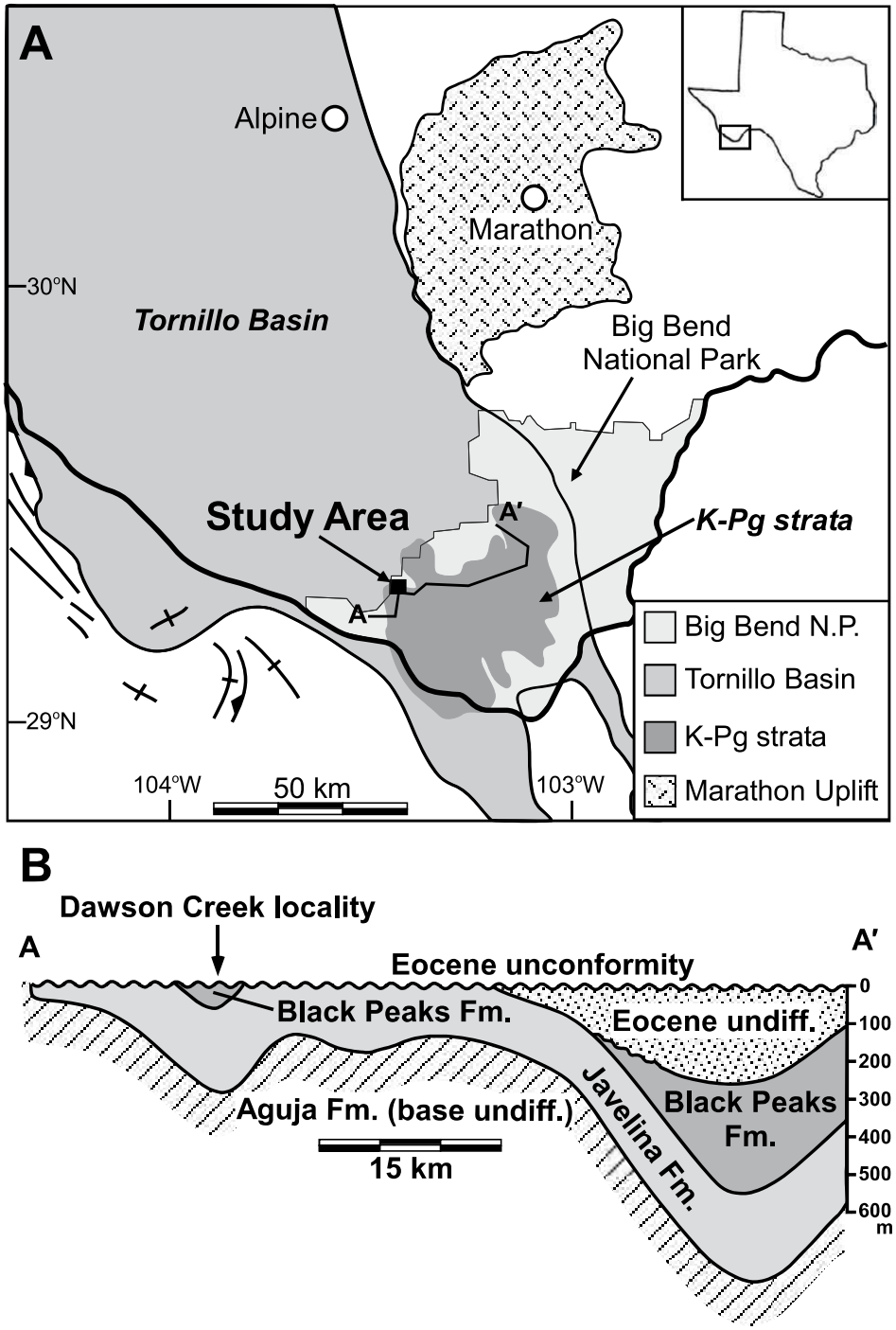

Figure 1. (A) Location of study area (highlighted with box) within Big Bend National Park (N.P.), modified from Lehman (1991). K-Pg—Cretaceous-Paleogene. (B) Cross-section A-A′ through the Tornillo Basin, modified from Lehman (1986).

of local isotope stratigraphy to marine isotope curves to produce a chronostratigraphic framework for the Dawson Creek area (e.g., Lehman, 1990; Nordt et al., 2003; Atchley et al., 2004). The existing age determinations indicate that the section spans from the latest Campanian through the early Paleocene (Nordt et al., 2003), when adjusted to reflect the most recent age of the Cretaceous-Paleogene boundary (e.g., Renne et al., 2013; Clyde et al., 2016). The Aguja Formation elsewhere in the park is interpreted to be stratigraphically equivalent to the base of the Dawson Creek section and contains a late Campanian vertebrate fauna (Rowe et al., 1992; Lehman, 1985; Wick and Lehman, 2013). Based on this correlation, the base of the Dawson Creek section has been interpreted to be close to the Campanian-Maastrichtian boundary (Lehman and Busbey, 2007). Based on the last occurrence of dinosaur fossils and the first occurrence of Paleocene mammals, the Cretaceous-Paleogene boundary has traditionally been identified in the Dawson Creek section to be at approximately the contact between the Javelina and Black Peaks Formations (Lehman, 1990). However, recent ichnological work documented an abrupt decrease in adhesive meniscate burrow diameter within a sandstone channel of the Javelina Formation at 172 m in the Dawson Creek section, which was interpreted to represent the postextinction recovery community, and thus the stratigraphic position of the Cretaceous-Paleogene boundary (Fig. 2; Wiest et al., 2018). Lehman (1990) used preliminary magnetostratigraphy (MacFadden *in* Standhardt, 1986) to argue that the Black Peaks Formation correlated to chrons C29r-C28r, meaning that the top of the section is older than 64.6 Ma, which is the end of C28r (Ogg, 2012). Correlations between stable isotopic trends from pedogenic carbonate nodules through the Dawson Creek section and carbon isotopes from marine deposits, combined with the location of cyclostratigraphic boundaries, were used to indicate the presence of multiple hiatuses in the section (Nordt et al., 2003; Atchley et al., 2004). However, the durations of these unconformities or their exact ages are uncertain.

There was a preliminary attempt to use magnetostratigraphy at Dawson Creek by B.J. MacFadden (*in* Standhardt, 1986) to determine the age of the section. In this work, the local polarity stratigraphy that was developed was correlated to C30n through C28r. However, MacFadden (*in* Standhardt, 1986) noted that large parts of the section were overprinted, and as a result, this magnetostratigraphic framework has not been accepted, though it was used by Lehman (1990) to estimate an approximate minimum age for the top of the section.

In other areas of the park, volcanic deposits within the upper portion of the Aguja Formation have been dated to 76.9 ± 1.2 Ma (Befus et al., 2008) and 72.6 ± 1.5 Ma (Breyer et al., 2007) using U-Pb dating, suggesting the Aguja Formation is Campanian in age. A monazite U-Pb age of 69.0 ± 0.9 Ma for a tuff occurring within the Javelina Formation, 90 m stratigraphically below the Cretaceous-Paleogene boundary, from the northern part of Big Bend National Park indicates that all, or at least the majority, of the Javelina Formation was deposited during the Maastrichtian (Lehman et al., 2006).

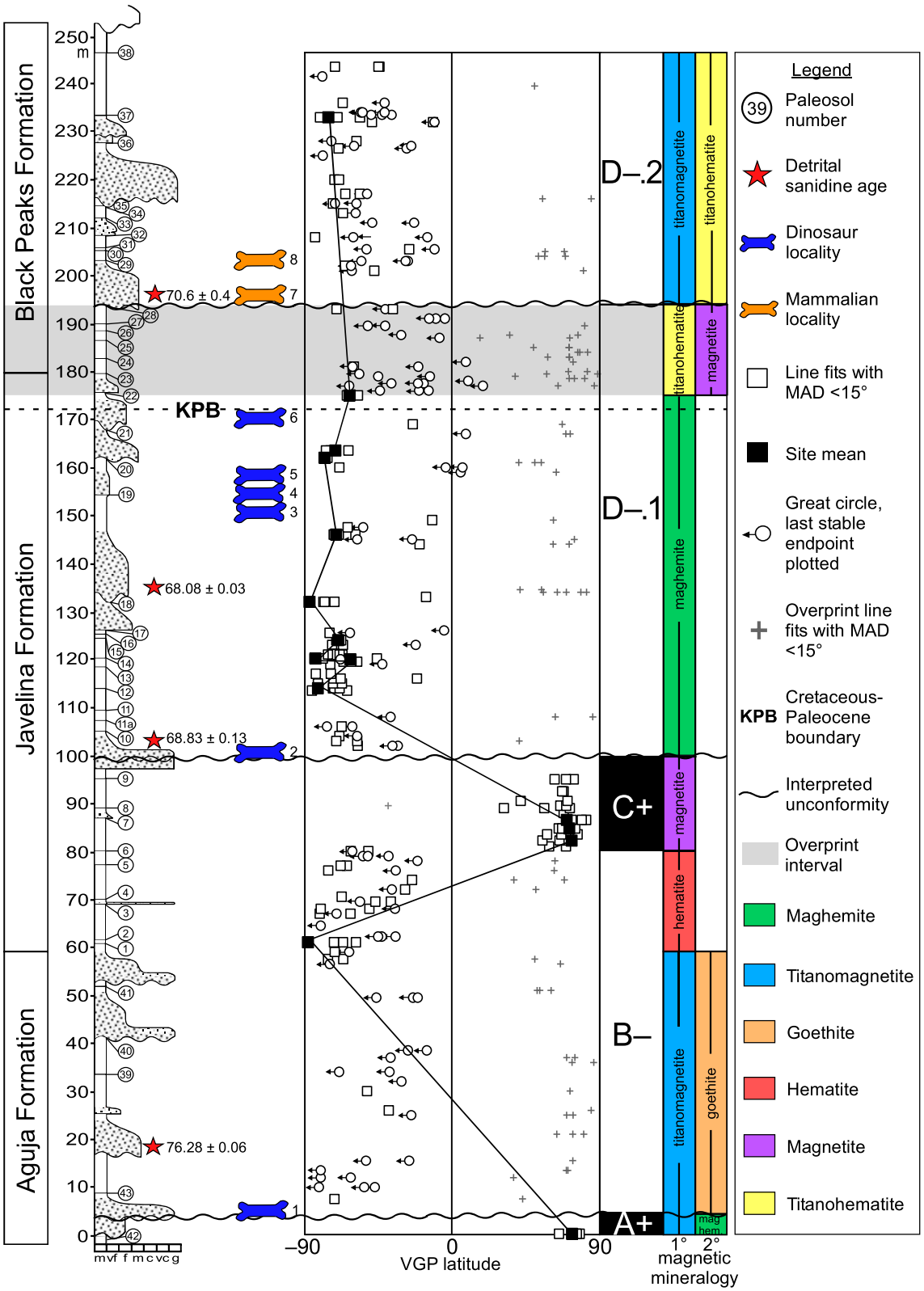

Figure 2. Virtual geomagnetic pole (VGP) latitude, interpreted polarity zonations, and primary (1°) and secondary (2°) magnetic mineralogies for the section. Locations of detrital sanidine samples are shown. Faunal localities: 1—LSU VL-110; 2—LSU VL-149; 3—TMM 41450 (LSU VL-106); 4—LSU VL-112; 5—LSU VL-145; 6—TMM 41501; 7—TMM 41400, "Tom's Top" (LSU VL-111); 8—LSU VL-109 (Lehman, 1990). Unconformities are placed based on sedimentological indicators, faunal interpretations, and detrital age dates. KPB—Cretaceous-Paleogene boundary; MAD—mean angle of deviation. Grain sizes: m—mud, vf—very fine sand, f—fine sand, m—medium sand, c—coarse sand, vc—very coarse sand, g—gravel.

Paleoclimate and Depositional Environments

Previous geochemical research that focused on paleosols through the succession documented two Late Cretaceous greenhouse events using the isotopic composition of pedogenic carbonate nodules, referred to as the mid-Maastrichtian event and late Maastrichtian event (Nordt et al., 2003). This work used correlations of the local isotope stratigraphy with marine isotope curves to adjust the ages of these events. When adjusted to reflect the most recent age of the Cretaceous-Paleogene boundary (Ogg, 2012; Renne et al., 2013), the mid-Maastrichtian event occurred from ca. 71 to 70 Ma, and the late Maastrichtian event occurred from ca. 66.2 to 66.3 Ma. Work done by Lehman (1990) on the Paleocene paleosols found a transition toward increased rainfall and cooler temperatures using paleosol macromorphology.

Alluvial stacking pattern analyses of the Aguja, Javelina, and Black Peaks Formations indicated that deposits in the Dawson Creek area were deposited cyclically (Atchley et al., 2004). Changes in stacking pattern thicknesses were interpreted to represent the rate of change of base-level rise and fall and to suggest that the primary control on stratigraphic cyclicity in the Dawson Creek section was eustatic sea-level change, despite the succession being deposited exclusively in the continental realm (Atchley et al., 2004). Interestingly, despite evidence for shifts in climate through the section, there does not appear to be evidence for climate change strongly influencing deposition (Atchley et al., 2004), which differs from evidence from other parts of the Big Bend area (Bataille et al., 2016).

Vertebrate Paleontology

Fossil vertebrates have been collected from the Big Bend National Park area for over 70 yr, and the Dawson Creek area contains a record of terrestrial vertebrate fossil localities throughout the Javelina and Black Peaks Formations. These faunas are of particular interest because they represent the southernmost latest Cretaceous and early Paleocene faunas of North America, and thus they are important for understanding terrestrial vertebrate biogeographic patterns across the Cretaceous-Paleogene boundary.

Disagreement on the placement of the formational boundaries between these units has resulted in differences in the taxa reported from each of the formations (e.g., Standhardt, 1986; Lehman, 1990; Rowe et al., 1992). For example, Standhardt (1986) considered the Javelina and Black Peaks units to be members of the Tornillo Formation and placed the Javelina–Black Peaks boundary above the mammal-bearing localities discussed here. Herein, we use the stratigraphic nomenclature and position of formational contacts of Lehman (1990), Nordt et al. (2003), and Atchley et al. (2004). Thus, we place all Paleocene mammal localities within the Black Peaks Formation, and all dinosaur faunas within the Javelina and Aguja Formations.

Aguja Formation

The Aguja Formation contains a rich vertebrate fauna that includes microvertebrate fossils collected through screen-washing techniques. These include chondrichthyan and actinopterygian fish (Rowe et al., 1992; Sankey, 1998; Standhardt, 1986), amphibians (Rowe et al., 1992; Lehman, 1985; Sankey, 1998; Standhardt, 1986), squamates (Rowe et al., 1992; Sankey, 1998; Standhardt, 1986; Nydam et al., 2013), turtles (Rowe et al., 1992; Sankey, 2008; Standhardt, 1986; Tomlinson, 1997), crocodylians (Colbert and Bird, 1954; Lehman, 1985; Rowe et al., 1992; Sankey, 2008; Standhardt, 1986), pterosaurs (Rowe et al., 1992), dinosaurs (Davies, 1983; Forster et al., 1993; Larson and Currie, 2013; Lehman, 1982, 1985, 1989b, 2010; Longrich et al., 2010, 2013; Prieto-Márquez, 2014; Rivera-Sylva et al., 2016; Rowe et al., 1992; Sankey, 1998, 2001, 2008; Sankey et al., 2005; Standhardt, 1986; Wagner, 2001; Wagner and Lehman, 2009; Wick et al., 2015), and mammals (Cifelli, 1995; Rowe et al., 1992; Weil, 1992).

Nearly all the seemingly valid dinosaur taxa identified from the Aguja Formation appear to be endemic. Several of the taxa, such as *Texacephale* (see Jasinski and Sullivan, 2011), are probably not valid. Several small theropod taxa that are based on isolated teeth (e.g., *Saurornitholestes langstoni*, *Richardoestesia gilmorei*, and *Richardoestesia isosceles*; Sankey, 2001, 2008) have been identified in temporally and geographically wide-ranging faunas throughout western North America, though it is likely that many, if not most of these, are not correctly identified, because small theropod taxa were probably exclusive to discrete time intervals and geographic areas (Larson and Currie, 2013).

Mammals from the Aguja Formation include several genera that are typical of Late Cretaceous faunas of western North America (e.g., *Alphadon*, *Turgididon*, *Pediomys*; Rowe et al., 1992). One species, the multituberculate *Cimolomys clarki*, indicates that the Aguja mammalian fauna correlates to the Judithian North American Land Mammal age (NALMA; Cifelli et al., 2004).

Javelina Formation

In the Dawson Creek area, a relatively small vertebrate fauna has been reported from the middle and upper Javelina Formation, and fossil specimens tend to be fragmentary, though bone beds containing multiple dinosaurs have been documented within the Javelina Formation in other areas of Big Bend National Park (Hunt and Lehman, 2008). The Javelina fauna includes the giant pterosaur *Quetzalcoatlus* from TMM 41501 in Dawson Creek (Table 1; Fig. 2; Lawson, 1975), and a number of dinosaurs, detailed next.

At least one chasmosaurine ceratopsian, *Bravoceratops polyphemus*, is present in the Javelina Formation of the Big Bend area, based on fragmentary specimens (Wick and Lehman, 2013), and this was regarded as being near in age to the Edmontonian-Lancian boundary. Fragmentary skulls and partial skeletons from the middle and upper Javelina Formation have been referred to, or tentatively referred to, *Torosaurus utahensis* (Lawson, 1976; Lehman, 1998; Hunt and Lehman, 2008), a taxon originally described from the North Horn Formation of Utah (see Sullivan et al., 2005). At least one taxon of a large titanosaurian sauropod has been identified from the Javelina Formation. Many of the sauropod specimens lack diagnostic characters to allow generic identification, but at least some can be confidently referred to *Alamosaurus sanjuanensis* (Lehman and Coulson, 2002; Fronimos and Lehman, 2014; Tykoski and Fiorillo, 2016). Some specimens of a large titanosaurian sauropod, probably representing *Alamosaurus*, have been described from the TMM 41450 (LSU VL-106) locality within the Javelina Formation

TABLE 1. DAWSON CREEK FOSSIL LOCALITIES

Locality	Taxa	Age
1. LSU VL-110	*Odontaspis* tooth, fish, crocodile, dinosaur	Lancian
2. LSU VL-149	*Tyrannosaurus* femur	Lancian
3. LSU VL-106, TMM 41450	*Alamosaurus sanjuanensis*	Lancian
4. LSU VL-112	Fish, turtle, crocodile	Lancian
5. LSU VL-145	Scraps of dinosaur bone	Lancian
6. TMM 41501	Giant pterosaur, *Quetzalcoatlus northropi*	Lancian
7. TMM 41400 "Tom's Top" (LSU VL-111)*	*Bryanictis*	Torrejonian
	Mixodectes malaris	Torrejonian 2
	Plesiolestes nacimienti	Torrejonian
	Promioclaenus cf. *P. lemuroides*	Torrejonian
8. LSU VL-109	Turtle remains	Torrejonian

*Taxa reclassified in this paper.

in the Dawson Creek section (Table 1; Fig. 2; Lawson, 1972; Standhardt, 1986), as well as near the top of the Cretaceous part of the section of the Rough Run area, which is near Dawson Creek (Fronimos and Lehman, 2014). A large tyrannosaurid, referred to *Tyrannosaurus rex* (Carr and Williamson, 2000, 2004), is present based on isolated postcranial bones (Wick, 2014) and on a partial maxilla (Lawson, 1975; Wick, 2014). At least two small theropod dinosaurs have been documented based on isolated teeth: *Saurornitholestes* cf. *S. langstoni* and *Sauronitholestes* n. sp.? (Sankey et al., 2005). Other dinosaurs reported from the Javelina Formation, but not well documented, are indeterminate hadrosaurs, ankylosaurs, and ornithomimids (Lawson, 1972; Lehman, 1985, 1990).

Several workers have reported that Lancian-age mammals and herpetofaunas are present in the Javelina Formation, citing Standhardt (1986). Standhardt (1986) reported a small microfauna from LSU locality VL-113 ("Running Lizard") in the Dawson Creek area, which she described as being from the upper Aguja Formation; however, based on its stratigraphic position, it is more likely from the Javelina Formation. She indicated a Lancian age for the fauna based on the presence of a fragmentary tooth that she referred to *Alphadon marshi*, a taxon restricted to the Lancian NALMA (Cifelli et al., 2004). However, we find that the tooth fragment is too incomplete to be diagnostic to genus or species.

The Javelina dinosaur fauna has been included in the latest Cretaceous "*Alamosaurus* community" (Sloan, 1969) or "*Alamosaurus* fauna" (Lehman, 1987), based primarily on the presence of the titanosauriform sauropod *Alamosaurus*, which is absent from contemporaneous latest Cretaceous faunas of the northern Rocky Mountain region. Lehman (1987) argued that *Alamosaurus* was confined to seasonal, semiarid intermontane basins south of ~35°N latitude, unlike the contemporaneous "*Triceratops* fauna," which was not environmentally restricted (Lehman, 1987). However, other workers have argued that the distribution of *Alamosaurus* does not reflect latitudinal faunal provinciality, but instead may be related to differences in ages between the *Alamosaurus* fauna of southern North America and the *Triceratops* fauna from the Northern Great Plains, or due to other environmental factors such as distance from the shoreline, with *Alamosaurus* restricted to more "inland" environments (e.g., Mannion and Upchurch, 2011; Lucas et al., 2016). Therefore, given the limited extent of the *Alamosaurus* fauna, determining the precise age of the Javelina Formation is of interest to further understanding possible latitudinal faunal provinciality or environmental heterogeneity during the latest Cretaceous of North America.

Black Peaks Formation

The Black Peaks Formation contains a diverse vertebrate fauna that includes a ray, a gar, amphibians, lizards, a champsosaur, turtles, crocodiles, and mammals (Schiebout, 1974; Schiebout et al., 1987; Standhardt, 1986; Brochu, 2000; Lehman and Barnes, 2010; Cobb, 2016).

The mammalian fauna found in the Black Peaks Formation has long been recognized as being Paleocene in age (e.g., Schiebout, 1974; Schiebout et al., 1987; Standhardt, 1986), based on the presence of diagnostic Torrejonian, Tiffanian, and possibly Clarkforkian NALMA taxa. In the Dawson Creek area, there are two mammalian fauna localities within the Black Peaks Formation: TMM 41400 (LSU VL-111; "Tom's Top"; Fig. 2) in Dawson Creek and TMM 42327 (LSU VL-108; "Dogie") from nearby Rough Run Amphitheater ~5 mi (8 km) east of the Dawson Creek section (Lehman and Busbey, 2007; Cobb, 2016). TMM 41400 and TMM 42327 localities have both yielded diverse microvertebrate assemblages that are 20 m and 80 m above the highest occurrence of dinosaur bones in those areas, respectively (see Lehman and Busbey, 2007; Cobb, 2016). Standhardt (1986) and Schiebout et al. (1987) described or provided a faunal list of several mammalian taxa recovered from low in the Black Peaks Formation that included a combination of Puercan and Torrejonian genera and species, leading them to conclude that these faunas are late Puercan. However, some workers have argued that those faunas are not Puercan, but Torrejonian in age (Williamson, 1996; Lehman and Busbey, 2007).

METHODOLOGY

Paleomagnetism

Four paleomagnetic block samples were collected from paleosols and fine-grained sandstones at ~1 m intervals (0.3 m minimum and 2 m maximum sample spacing) through the section. In total, 121 localities were sampled. A flat face was shaved onto the samples *in situ* using a hand rasp, and the orientation was measured using a Brunton compass. In the laboratory, the samples were cut into ~2 cm^3 cubes using a diamond-bit saw.

In total, 360 samples were measured at Baylor University using a 2G cryogenic DC-SQuID magnetometer located in a two-layer magnetostatic shielded room with a background field typically less than 300 nT. A dip correction was applied to the section based on field measurements ranging from 14° to 36°. All samples were demagnetized using a combined alternating field (AF) and thermal demagnetization strategy following the methods of Peppe et al. (2009). Samples were first given a low-AF pretreatment (50 and 100 MT steps) to remove any low-coercivity viscous or isothermal remanence. Thermal demagnetization steps were performed in 20°–50° increments up to the maximum unblocking temperature or until samples became erratic and unstable (between 250 °C and 600 °C). Thermal demagnetization was performed using a nitrogen atmosphere with an ASC (Carlsbad, California) controlled atmosphere thermal demagnetizer to minimize oxidation reactions.

The characteristic remanence for samples was isolated using principal component analysis (PCA; Kirschvink, 1980). A best-fit line was calculated from a minimum of three demagnetization steps that trended toward the origin and had a maximum angle of deviation (MAD) <20° (Figs. 3A, 3B, and 3C). Specimens that were analyzed by great circles were used if they had a MAD <20° (Fig. 3D). Virtual geomagnetic pole directions for circles were calculated using their last stable end point used in the great circle calculation. Data from specimens that had erratic demagnetization behaviors were excluded from analysis (Fig. 3E). A site mean direction was calculated for all sites having three samples with statistically significant directions using Fisher statistics (Fisher, 1953). Only sites that passed the Watson test for randomness (Watson, 1956) were used. Reversal boundaries were placed at the stratigraphic midpoints between samples of opposing polarity. The local polarity stratigraphy was then correlated to the geomagnetic polarity time scale (GPTS; Ogg, 2012).

Rock Magnetism

Rock magnetic analyses were performed at the Institute for Rock Magnetism at the University of Minnesota, Minneapolis, Minnesota. High-temperature susceptibility measurements were collected on eight rock samples using a Geofyzika KLY-2 Kappabridge AC (Brno, Czech Republic) susceptibility meter in air. Measurements were recorded on warming from room temperature to 650 °C and on cooling back to room temperature. The first derivative of the measurements was used to determine the Curie temperatures. Hysteresis loops were measured on a MicroMag Princeton Measurements (Princeton, New Jersey) vibrating sample magnetometer (VSM) on eight samples at temperatures ranging from 30 °C to 600 °C.

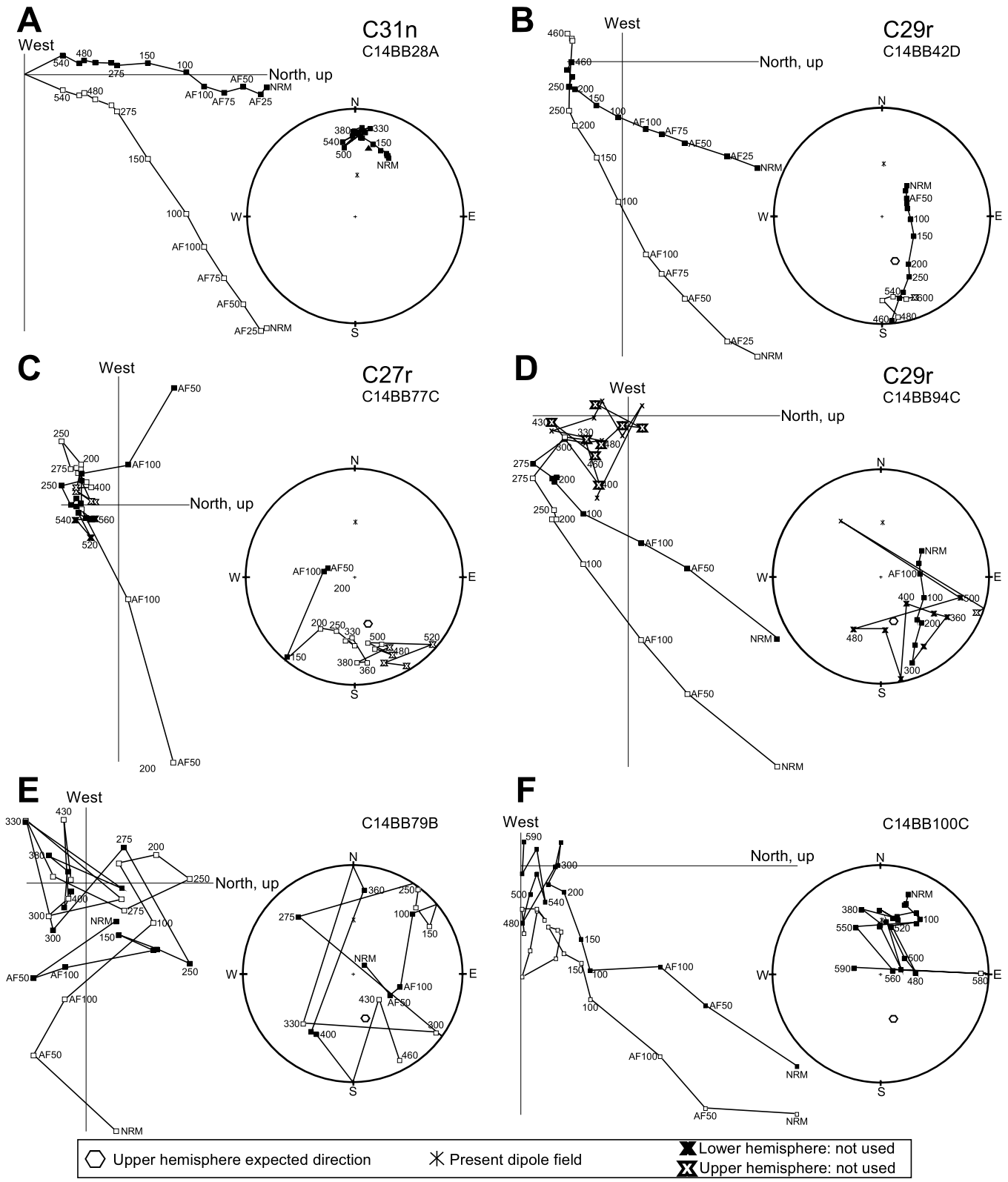

Figure 3. Representative Zijderveld diagrams and equal-area plots for each subset of data. (A) Demagnetization trajectory of a normal polarity sample from C31n where a line was calculated (36% of data). (B) Demagnetization trajectory of reversed polarity sample from C29r where a line was calculated. (C) Demagnetization trajectory of a reversed polarity sample from C27r where a line was calculated. (D) Reversed polarity sample with demagnetization trajectory best characterized by a great circle from C29r, where direction was calculated from last stable end point (28% of the data). Sample is located in overprinted interval. (E) Representative sample of erratic data that were not used for interpretations (11% of data). (F) Representative overprinted sample where calculated direction overlaps with modern (25% of data). NRM—natural remanent magnetization.

The Quantum Design Magnetic Properties Measurement System (MPMS; San Diego, California) was used for low-temperature remanence measurements on eight samples. The protocol included field-cooled (FC) remanence, zero-field-cooled (ZFC) low-temperature saturation isothermal remanent magnetization (LTSIRM), and room-temperature saturation isothermal remanent magnetization (RTSIRM) following the methods of Sprain et al. (2016). This method involves initially applying a sustained direct current (DC) field of 2.5 T on a sample as it cools from 300 K to 20 K (FC). The field is then turned off, and remanence is measured while the sample warms to 300 K. The sample is cooled back down to 20 K with no field applied (ZFC), after which a 2.5 T LTSIRM is applied. Remanence is measured while the sample warms back to 300 K. While at 300 K, a 2.5 T SIRM (RTSIRM) is applied, and the remanence is measured while cooling down to 20 K and then warming to 300 K.

Detrital Sanidine Dating

Four samples were collected in the field from channels within the Aguja, Javelina, and Black Peaks Formations. Sample SS02 was taken at the base of the channel above paleosol 23 (Fig. 2). Samples SS07 and SS08 were taken within the Javelina Formation from the top of the channel below P10 and from the base of the channel below paleosol 19, respectively (Fig. 2). Sample SS13, from the Black Peaks Formation, was taken at the base of the channel above paleosol 28.

All processing and mineral separations were done at the New Mexico Geochronology Research Laboratory (NMGRL), Socorro, New Mexico. Sample separation included: crushing and grinding whole rocks, cleaning with H_2O and HF acid, and sieving to appropriate grain size. Magnetic and heavy liquid density separation techniques were used to concentrate the K-feldspar grains. Sanidine was handpicked from the bulk feldspar separate based on optical clarity as viewed under a binocular microscope. As shown later by the argon analyses, the picked clear grains contained significant plagioclase and quartz.

The sample crystals were irradiated at the TRIGA reactor in Denver, Colorado, for 16 h in the NM-276 package along with Fish Canyon sanidine interlaboratory standard FC-2, with an assigned age of 28.201 Ma (Kuiper et al., 2008). Ages were calculated with a total ^{40}K decay constant of $5.463e^{-10}$/yr (Min et al., 2000).

After irradiation, six crystals of FC-2 from each monitor hole and ~100 sample crystals were loaded into copper trays, evacuated, and baked at 140 °C for 4 h. Sample crystals were fused with a CO_2 laser, and the extracted gas was cleaned with an NP 10 getter operated at 1.5 A for 30 s. The gas was analyzed for argon isotopes using an ARGUS VI (Breman, Germany) multicollector mass spectrometer equipped with five Faraday cups, and one ion counting multiplier (compact discrete dynode [CDD]). The configuration had ^{40}Ar, ^{39}Ar, ^{38}Ar, ^{37}Ar, and ^{36}Ar on the H1, AX, L1, L2, and CDD detectors, respectively. All data acquisition was accomplished with New Mexico Tech Pychron software, and data reduction used Mass Spec (v. 7.875), written by Al Deino at the Berkeley Geochronology Laboratory. Extraction line blank plus mass spectrometer background data are given in Table DR3.[1]

Minimum age populations were generally defined by choosing the youngest dates that formed a normal distribution as defined by the mean square of weighted deviates (MSWD) value of the distribution. The minimum age was taken as the inverse variance weighted mean of the selected crystals, and the error is given as the square root of the sum of $1/\sigma^2$ values. The error was also multiplied by the square root of the MSWD for MSWD values greater than 1. The *J*-error is included for all weighted mean ages, and all errors are reported at 1σ unless otherwise noted.

Vertebrate Paleontology

A description and reevaluation of the therian component of the mammalian faunas, which is primarily based on isolated and often fragmentary teeth, was undertaken by detailed examination of the specimens collected by Schiebout, Standhardt, and collaborators from the TMM 41400 (LSU VL-111; Tom's Top; Fig. 2), TMM 42327 (LSU VL-108; Dogie), and other localities from Big Bend (Schiebout, 1974; Schiebout et al., 1987; Standhardt, 1986). We also reevaluated the taxonomy of the Cretaceous dinosaur faunas from the Javelina and Aguja Formations.

RESULTS

Magnetostratigraphy

In total, 360 samples were analyzed from 121 sampling horizons. The samples can be divided into four subsets based on demagnetization behavior. The demagnetization trajectory of 36% of samples began with a strong north and moderately downward overprint that was mostly removed by ~275 °C (Fig. 3A) up to 450 °C (Figs. 3B and 3C), after which the stable end point was reached. The second subset, encompassing 28% of samples, had a demagnetization trajectory that was best characterized by a great circle. For these samples, the latitude and longitude of the virtual geomagnetic pole (VGP) were calculated using the last coherent direction along a great circle trajectory (Fig. 3D), which was usually not a stable end point, but which was sufficient to define polarity. The third subset of samples, 11% of samples, had an erratic demagnetization trajectory, from which a good direction could not be calculated (Fig. 3E). These samples were not used for polarity interpretation. The fourth subset, consisting of the remaining 25% of samples, had a stable direction between 100 °C and 300 °C, which then became erratic (Fig. 3F). The VGPs of these samples consistently overlapped with the modern direction, and they were interpreted to be completely overprinted. Consequently, these samples were not used for polarity interpretation.

In total, 235 samples from 121 sampling horizons composed the first and second subsets and were used to calculate directions (Fig. 4; Table 2; Tables DR4 and DR5 [see footnote 1]). Site mean directions were calculated from 15 sample horizons that had three samples with statistically significant directions and passed the Watson test for randomness (Watson, 1956; see also Table DR6 [see footnote 1]). The mean VGP latitude and longitude for Late Cretaceous reversed samples (local polarity B–) was –88°N, 274.7°E (n = 23; a_{95} = 12.1), and mean VGP latitude and longitude for normal samples (local polarity A+, C+) was 76.4°N, 26.7°E (n = 30, a_{95} = 7.3). The mean VGP latitude and longitude for Cretaceous–Paleogene samples (D–.1) was –79.5°N, 288.2°E (n = 57, a_{95} = 6.3). The mean VGP latitude and longitude for early Paleocene samples (D–.2) was –76.9 °N, 191.6°E (n = 21, a_{95} = 12.8). These pole locations are significantly distinct from the Cretaceous and Paleocene reference paleomagnetic pole for North America (Fig. 4; Torsvik et al., 2008). There was also a small but consistent clockwise directional offset from the expected direction, which had no effect on our polarity interpretations. The origin of the directional offset and the difference between our calculated VGPs and the Cretaceous and Paleocene reference poles are likely due to variability in dip throughout the section, which may have been overcorrected for, and syndepositional or early postdeposition inclination shallowing, with a flattening factor of ~10%.

The local polarity stratigraphy shows each sample direction and site means (Fig. 2). Polarity zones A– through D–.2 are highlighted, along with interpreted hiatuses. An overprint

[1]GSA Data Repository item 2018042, argon data, line, circle, and site mean paleomagnetic data, and additional figures and detailed descriptions of therian mammals, is available at http://www.geosociety.org/datarepository/2018 or by request to editing@geosociety.org.

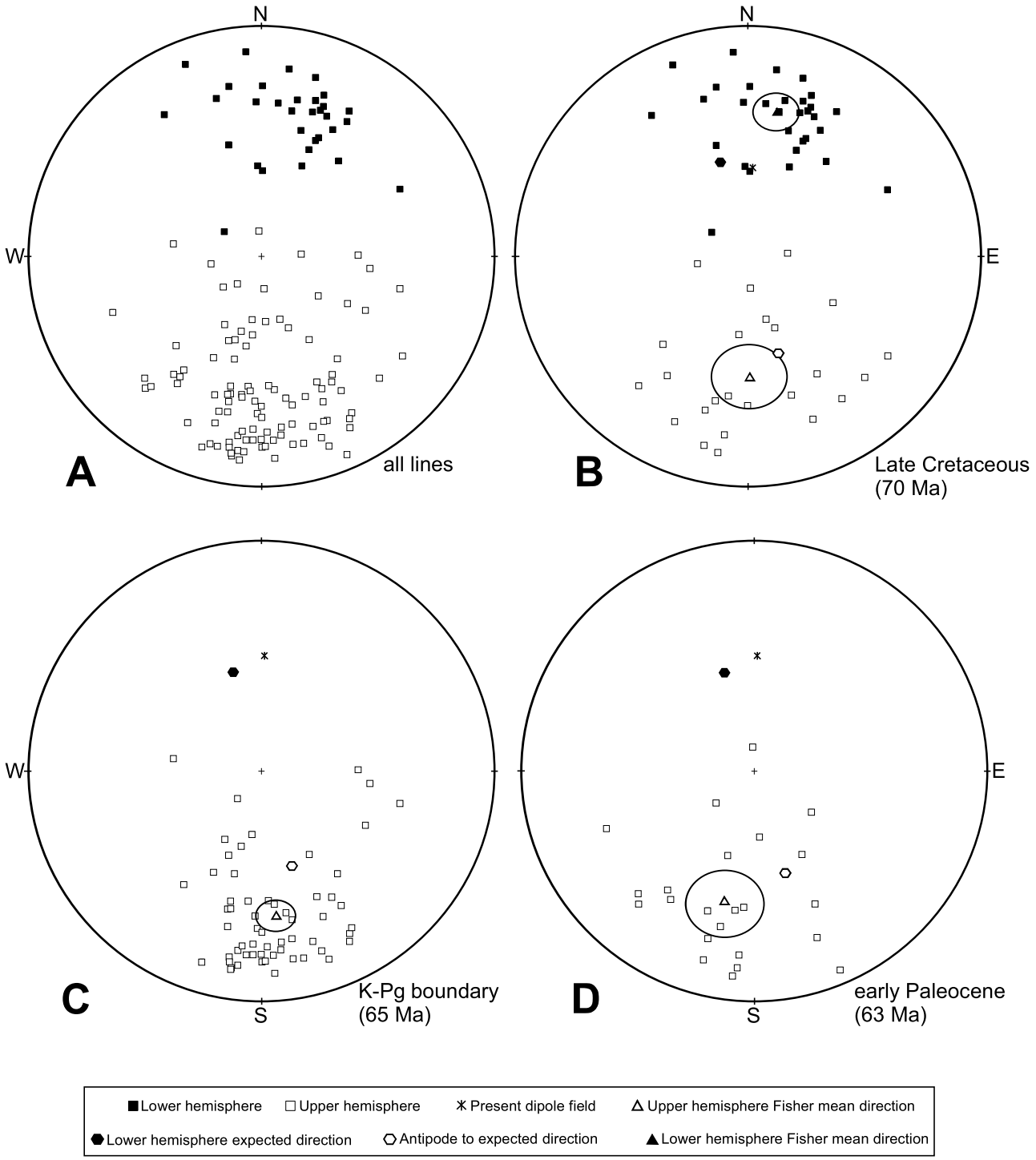

Figure 4. Equal-area plot of characteristic magnetization directions calculated from: (A) all lines; (B) all lines from Late Cretaceous interval; (C) all lines from Cretaceous-Paleogene (K-Pg) boundary interval; and (D) all lines from early Paleocene interval.

interval is present at the top of the Javelina Formation and the base of the Black Peaks Formation from 177 to 194 m (Fig. 2). In this interval, there is a high proportion of overprint line fits and great circles where the direction was calculated from the last stable end point.

Detrital Sanidine Dating

The detrital sanidine dates in this study were used to correlate the deposits to the GPTS and to constrain the maximum deposition age. The age probability plots for all samples and associated analytical results are provided in Figure 5. Figure 2 shows the stratigraphic position of each detrital sanidine sample.

The Aguja Formation sample, SS02, has a minimum age population (= maximum depositional age) of 76.28 ± 0.06 Ma. Two samples

TABLE 2. MEAN PALEOMAGNETIC DIRECTION DATA FROM THE DAWSON CREEK SECTION

Subset	*n*	*D* (°)	*I* (°)	*k*	a95 (°)	Pole (°N)	Pole (°E)	*K*	A95 (°)
C32n–lines	3	13.3	31.5	96.2	12.6	72.9	28.4	107.2	12.0
C31r–lines	23	179.3	–46.0	7.3	12.1	87.6	226.2	5.6	14.0
C31n–lines	27	11.4	36.8	12.4	8.2	77.3	19.0	11.1	8.7
C31n–sites	3	358.4	29.5	27.5	24.0	76.5	83.2	24.1	25.7
C29r–lines	58	173.1	–36.6	9.5	6.4	80.8	118.4	8.2	7.0
C29r–sites	9	178.7	–30.8	23.2	10.9	77.7	81.7	24.2	10.7
C27r–lines	21	192.9	–40.6	7.2	12.8	78.4	354.1	6.0	14.2

Note: n—number of lines or sites included in the mean; *D*—declination; *I*—inclination; *k*—Fisher's (1953) precision parameter; a_{95}—radius of 95% confidence cone around mean (Fisher, 1953); pole N and E—mean of virtual geomagnetic poles calculated from each line or site mean; *K* and A95—Fisher statistics of paleomagnetic pole.

were dated from the Javelina Formation, SS07 and SS08. Sample SS07 recorded a minimum age population of 68.83 ± 0.13 Ma, whereas, sample SS08 has a well-defined minimum age population at 68.08 ± 0.03 Ma. The sample from the Black Peaks Formation, SS13, has a minimum age population of 70.6 ± 0.4 Ma. However, the maximum depositional age is defined by a single grain dated to 65.9 ± 0.4 Ma.

Rock Magnetism

The dominant magnetic mineralogy in the Aguja Formation is a low-Ti titanomagnetite indicated by a 525 °C Curie temperature in high-temperature hysteresis loops and a Verwey transition at ~110 K, which is lower than expected for pure magnetite (Figs. 6A and 6B). High-temperature hysteresis loops for a normal polarity sample from the A+ interval of the Aguja Formation show a 600 °C Curie temperature, suggesting the presence of maghemite as well. FC/ZFC curves from low-temperature rock magnetometry for a reversed polarity sample from the B– interval of the Aguja Formation converge at 300 K, suggesting goethite is also a magnetic carrier.

Throughout the Javelina Formation, the dominant magnetic mineralogy varies. For the basal portion of the formation, samples with statistically significant reversed directions (B– interval) have >600 °C Curie temperatures measured from high-temperature susceptibility and hysteresis loops, which indicate hematite is the primary magnetic mineral (Figs. 6C and 6D). In the overlying C+ interval, low-temperature rock magnetometry measurements for a representative normal polarity sample show a pronounced Verwey transition at 120 K, with $M_{FC} > M_{ZFC}$ (M is magnetization), suggesting single-domain magnetite is the dominant magnetic carrier (Figs. 6E and 6F). Both high-temperature susceptibility measurements and hysteresis loops demonstrate a 600 °C Curie temperature, signaling maghemite is the dominant magnetic mineralogy over the D– interval of the Javelina Formation (Figs. 6G and 6H).

Large numbers of samples are interpreted to be overprinted in the upper portion of the Javelina Formation and lower portion of the Black Peaks Formation (Fig. 2). Rock magnetic analyses for a representative overprinted sample and representative reversed sample within this interval indicate that titanohematite is the dominant magnetic carrier, with minor amounts of magnetite. RTSIRM curves indicate an approximate twofold increase in remanence, which could suggest either goethite or titanohematite (Figs. 7A and 7C; Dekkers, 1989; France and Oldfield, 2000). However, FC-ZFC-LTSIRM curves also show little to no separation between FC and ZFC curves, which would be expected with goethite (Figs. 7B and 7D). Consequently, titanohematite is the most likely magnetic carrier.

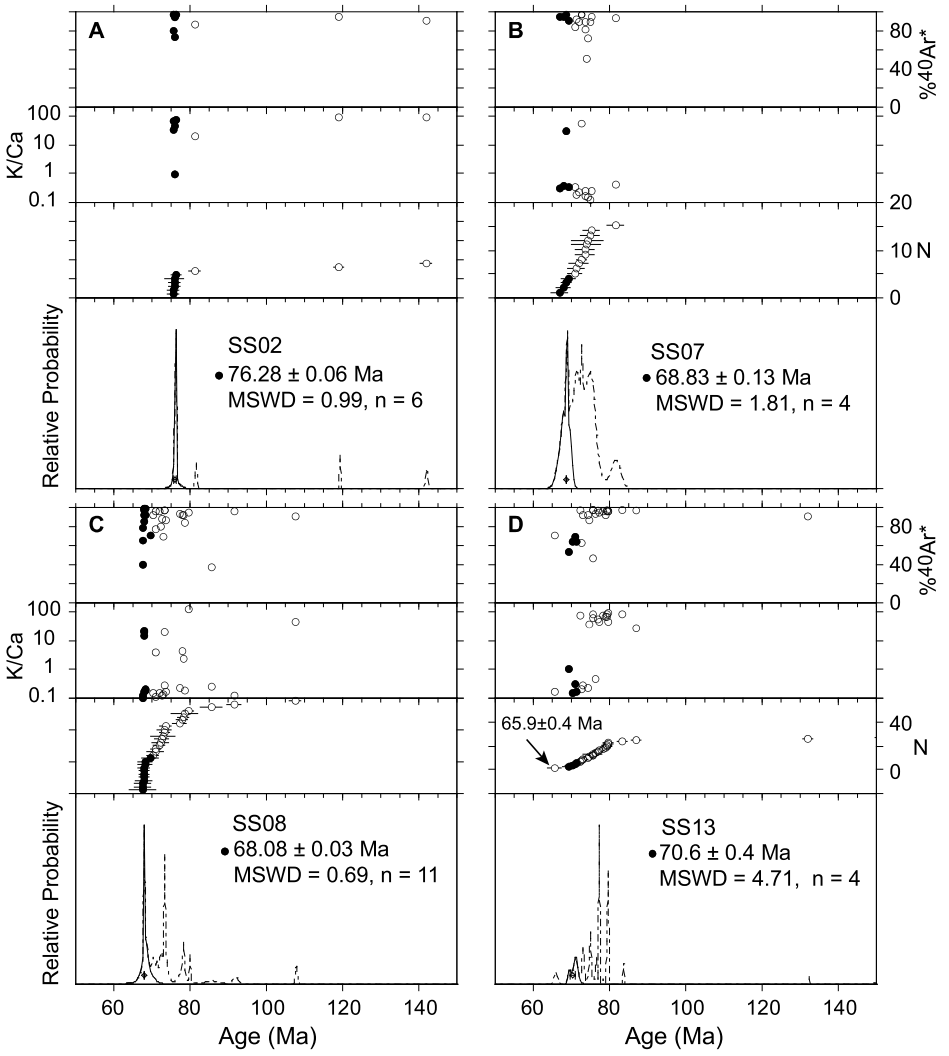

Figure 5. Age probability diagrams for the four analyzed samples: (A) SS02, (B) SS07, (C) SS08, and (D) SS13. The plots show, from bottom to top, the age probability distribution spectrum, where the dashed line represents the probability curve for all of the data, whereas the solid line is for the data shown with solid circles; distribution of individual single-crystal ages with 2σ errors (N); K/Ca ratios; and percentage of radiogenic ^{40}Ar. MSWD—mean square of weighted deviates.

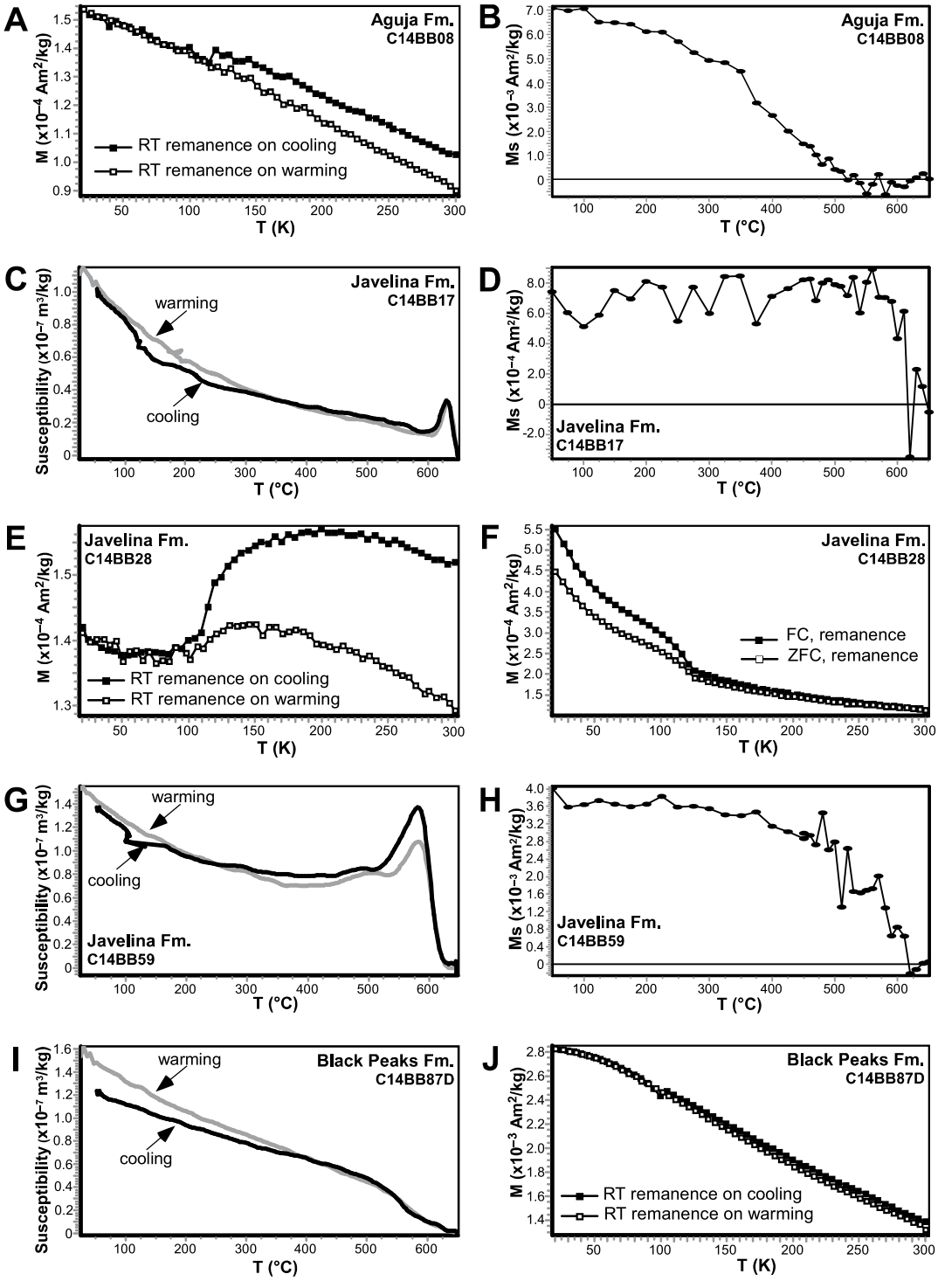

Figure 6. Rock magnetic analysis results, including low-temperature magnetization curve of representative samples, high-temperature vibrating sample magnetometer (VSM) curves of curves of saturation magnetization (Ms), and high-temperature heating and cooling curves of bulk magnetic susceptibility in air. Temperature given in Celsius (°C) above room temperature and Kelvin (K) below room temperature following Dunlop and Ozdemir (1997). M—magnetization. Room-temperature (RT) plots show magnetization measurements at room temperature following the application of saturation isothermal remanent magnetization (SIRM). Field-cooled (FC) and zero field-cooled (ZRC) plots show magnetization during warming following a sustained direct current field of 2.5 T during cooling (FC) and during warming following a SIRM imparted at low temperature (ZFC). (A) RT curves for a B– polarity zone reversed polarity sample from the Aguja Formation indicating titanomagnetite. (B) High-temperature VSM curve for a B– polarity zone reversed polarity sample from the Aguja Formation indicating titanomagnetite. (C) High-temperature susceptibility curves for a B– polarity zone reversed polarity sample in the Javelina Formation indicating hematite. (D) High-temperature VSM curve for a B– polarity zone reversed polarity sample in the Javelina Formation indicating hematite. (E) RT curves for a C+ polarity zone normal polarity sample in the Javelina Formation indicating magnetite. (F) FC/ZFC curves for a C+ polarity zone normal polarity sample in the Javelina Formation indicating magnetite. (G) High-temperature susceptibility curves for a D–.1 polarity zone reversed polarity sample in the Javelina Formation indicating maghemite. (H) High-temperature VSM curve for a D–.1 polarity zone reversed polarity sample in the Javelina Formation indicating maghemite. (I) High-temperature susceptibility curves for a D–.2 polarity zone reversed polarity sample in the Black Peaks Formation indicating titanomagnetite. (J) RT curves for a D–.2 polarity zone reversed polarity sample in the Black Peaks Formation indicating titanomagnetite.

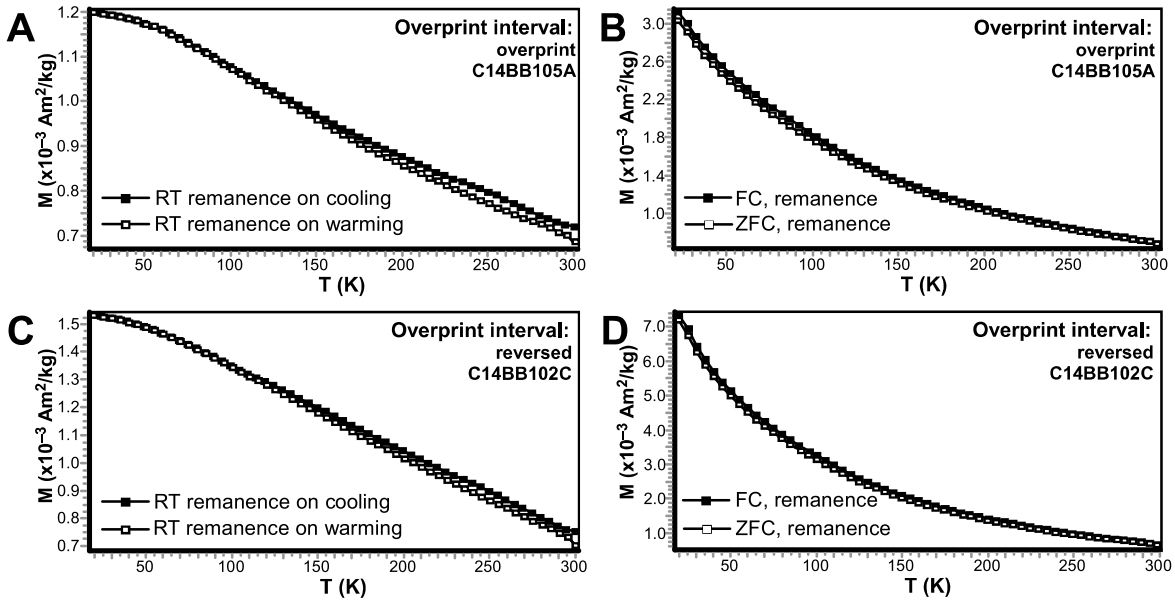

Figure 7. Rock magnetic analysis for the overprint interval in the upper Javelina and lower Black Peaks Formations indicating titanohematite. M—magnetization. (A) Room-temperature (RT) curves for an overprinted sample in the overprint interval. (B) Field-cooled (FC) and zero field-cooled (ZRC) curves for an overprinted sample in the overprint interval. (C) RT curves for a reversed sample in the overprint interval. (D) FC/ZFC curves for a reversed sample in the overprint interval.

This interpretation is further supported by the similar character of the curves to those interpreted as titanohematite by Sprain et al. (2016). Overprinted samples were differentiated from a Cretaceous-Paleogene normal polarity based on the presence of titanohematite and VGPs that overlapped with modern values.

Titanomagnetite is the dominant magnetic carrier in the Black Peaks Formation above the overprinted interval, as indicated by a 560 °C Curie temperature and 110 K Verwey transition in high-temperature susceptibility, low-temperature magnetometry, and high-temperature hysteresis loops (Figs. 6I and 6J). Titanohematite also appears to be a secondary magnetic carrier in this interval.

Vertebrate Paleontology

The results of a reevaluation of the lower Black Peaks Formation faunas of the Dawson Creek, Rough Run, and possibly correlative areas of Big Bend National Park are summarized in Figures 8 and 9, Table 3, and the Appendix. Mammals originally identified as Puercan NALMA taxa (i.e., *Eoconodon*, *Periptychus coarctatus* [= *Carsioptychus coarctatus*], and *Ellipsodon priscus*) were misidentified and instead represent typical and, in some cases, defining Torrejonian taxa (*Triisodon coryphaeus*, *Periptychus carinidens*, and *Ellipsodon* cf. *E. inaequidens*; Table 3). In addition, we describe two new species that are endemic to the Black Peaks Formation of Big Bend National Park (see Appendix).

The fauna from low in the Paleocene interval of the Dawson Creek section (TMM locality 41400 [LSU VL-111]; Tom's Top) can be confidently placed within the Torrejonian NALMA based on the presence of several characteristic Torrejonian taxa (see Lofgren et al., 2004): the genera *Bryanictis*, *Mixodectes*, *Plesiolestes*, and *Promioclaenus*. Moreover, two of these taxa are represented by species known only from the middle Torrejonian (To2), *Mixodectes malaris* and *Plesiolestes nacimienti*. *M. malaris* is an index taxon for the middle Torrejonian and is restricted to chron C27r of the Nacimiento Formation (Williamson, 1996), and it is also present in the Swain Quarry fauna of the Fort Union Formation of Wyoming (Rigby, 1980). *Promioclaenus lemuroides* is also tentatively identified in the fauna and is restricted to the Torrejonian of western North America, where it is present in Montana, Wyoming, Utah, and New Mexico.

The fauna from TMM 42327 (LSU VL-108; Dogie) of Rough Run Amphitheater is also firmly established to be Torrejonian because it contains the defining taxon for the Torrejonian: *Periptychus carinidens*. That fauna also contains a number of other taxa, including *Bryanictis*, *Ellipsodon*, and *Mioclaenus*, which are elsewhere restricted to the Torrejonian. *Ellipsodon* is from the middle Torrejonian (To2), and the species *Ellipsodon inaequidens*, which is tentatively identified in the Dogie fauna, is restricted to the lower part of chron C27r in the Nacimiento Formation, in the *Protoselene opisthacus–Ellipsodon granger* [Tj2] and *E. granger–Arctocyon ferox* [Tj3] zones (after Williamson, 1996).

Following the reevaluation of the Tom's Top and Dogie faunas, we find that no fossil therian mammals that are restricted to the Puercan are present in the Black Peaks Formation, and instead the fauna is composed of Torrejonian taxa. Thus, we can confidently correlate these fossil localities to the Torrejonian NALMA (Table 3; a complete description of the therian mammals from these localities is contained in the Appendix). Further, given the occurrence of taxa in both localities that are restricted to the middle Torrejonian in the San Juan Basin in New Mexico, we tentatively correlate both TMM 41400 (Tom's Top) and TMM 42327 (Dogie) to the Torrejonian 2 NALMA.

The reidentification of taxa from localities low in the Black Peaks Formation and reevaluation of the resulting biochronology of the Aguja, Javelina, and Black Peaks Formations indicate that the Aguja fauna correlates to the Judithian NALMA, the Javelina fauna correlates to the Lancian NALMA, and the Black Peaks fauna correlates to the Torrejonian. Therefore, there is likely a significant hiatus between the vertebrate localities in the Aguja Formation and the Javelina Formation and another major hiatus between the vertebrate localities in Javelina Formation and the Black Peaks Formation.

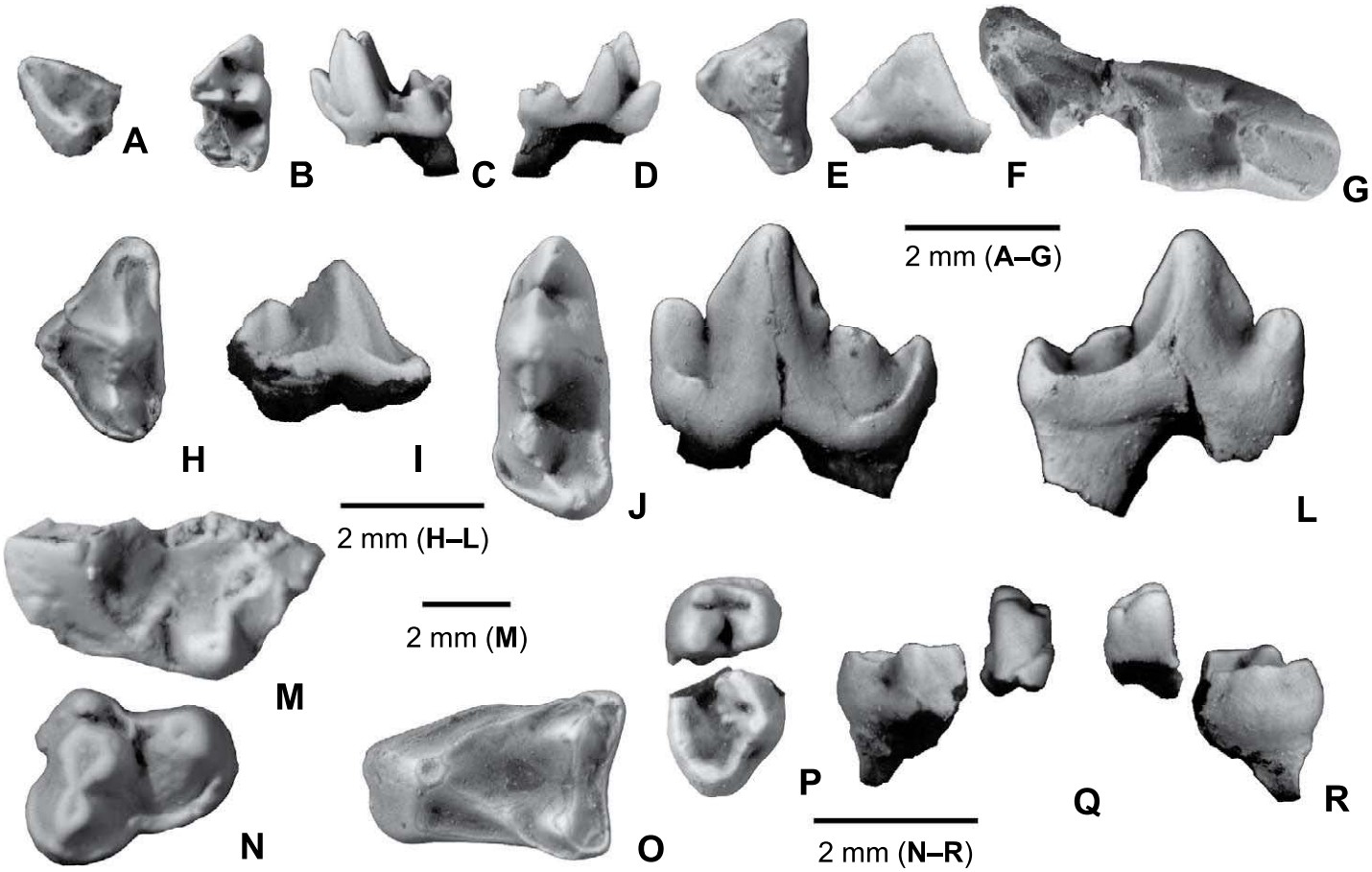

Figure 8. Metatheria, Cimolesta, Carnivoramorpha, and Euarchonta fossils from the Dawson Creek and Rough Run areas, Big Bend National Park, Texas. (A–D) *Peradectes* sp.: (A) partial right M1 (LSU V-895) in occlusal view; (B–D) left m2 or m3 (LSU V-705), in occlusal (B), buccal (C), and lingual (D) views; (E–G) Cimolestidae indeterminate: (E–F) left P3 (LSU V-708) in occlusal (E) and buccal (F) views; (G) partial right M2 (LSU V-841) in occlusal view; (H–I) *Bryanictis* new sp.: (H–I) left P3 (LSU V-709) in occlusal (H) and buccal (I) views; (J–L) left p4 (TMM 41400–10, holotype) in occlusal (J), buccal (K), and lingual (L) views; (M) *Mixodectes malaris*, partial left M3 (LSU V-924) in occlusal view; (N–R) *Plesiolestes nacimienti*: (N) right P4 (LSU V-921) in occlusal view, (O) left M2 (TMM 41400–17) in occlusal view, (P–R) partial right m3 (LSU V-923) in occlusal (P), buccal (Q), and lingual (R) views. Specimens have been dusted with magnesium oxide to increase visibility of surface features.

DISCUSSION

Magnetic Mineralogy

The dominant magnetic mineralogy of the Aguja and Black Peaks Formations is titanomagnetite. The Javelina Formation contains various magnetic mineralogies, including hematite, single-domain magnetite, maghemite, and titanohematite. The presence of titanohematite as a magnetic carrier can explain much of the overprint signal in the upper portion of the Javelina Formation and lower portion of the Black Peaks. Titanohematite is likely detrital and has a relatively low Curie temperature, ranging from 150 °C to 200 °C; consequently, the grains could easily be viscously reset with modest burial heating. The Black Peaks Formation in the section is overlain by basaltic flows, which plausi-

Figure 9 (*on following page*). "Condylarthra" fossils from the Dawson Creek and Rough Run areas, Big Bend National Park, Texas. (A–E) *Haploconus* sp.: (A) partial right M1 (LSU V-711) in occlusal view, (B) partial right M2 (LSU V-710) in occlusal view, (C–E) partial left m1 (LSU V-835) in occlusal (C), lingual (D), and buccal (E) views; (F–H) *Periptychus carinidens*: nearly complete m3 (LSU V-888) in occlusal (F), lingual (G), and buccal (H) views; (I–J) *Promioclaenus* cf. *P. lemuroides*: (I) left P3 (LSU-875) in occlusal view, (J) partial left M3 (LSU V-920) in occlusal view; (K–U) *Mioclaenus* new sp.: (K–L) left P4 (LSU V-833) in occlusal (K) and buccal (L) views, (M–N) left M1 (LSU V-891) in occlusal (M) and buccal (N) views, (O–P) left M2 (LSU V-890, holotype) in occlusal (O) and buccal (P) views, (Q–R) partially erupted right m2 (LSU V-703) in occlusal (Q) and lingual (R) views, (S–U) left m3 (LSU V-881) in occlusal (S), buccal (T), and lingual (U) views; (V–Z) *Ellipsodon* cf. *E. inaequidens*: (V–W) left M1 (LSU V-706) in occlusal (V) and buccal (W) views, (X–Z) right m1 (LSU V-701) in occlusal (X), buccal (Y), and lingual (Z) views; (AA–BB) cf. *Goniacodon levisanus*: (AA–BB) left M3 (LSU V-704) in occlusal (AA) and buccal (BB) views. Specimens have been dusted with magnesium oxide to increase visibility of surface features.

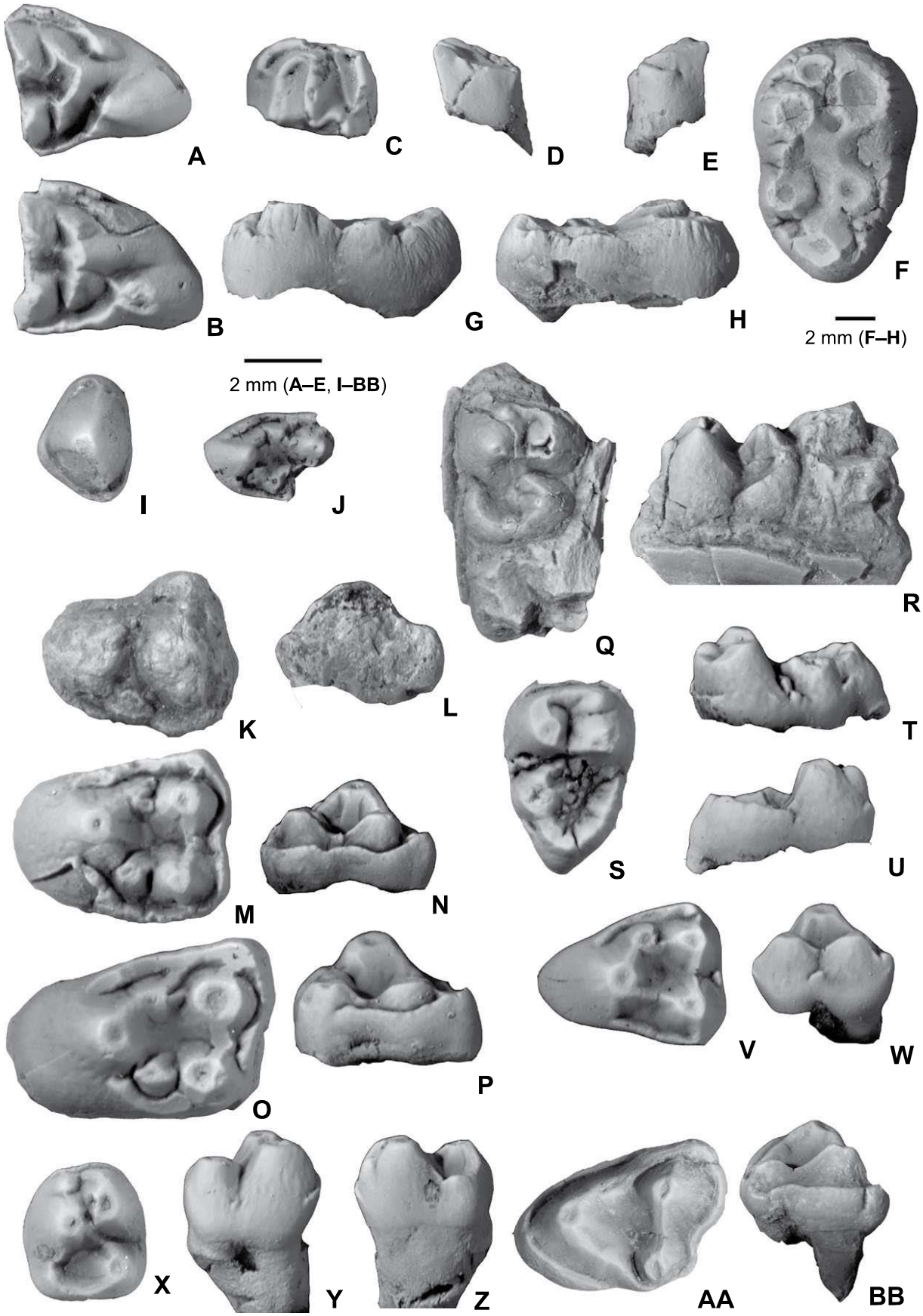

Figure 9.

TABLE 3. THERIAN MAMMALS

Standhardt (1986)	This paper
TMM locality 41400, "Tom's Top"	
Carnivora	Carnivoramorpha
Didymictidae	Viverravidae
Bryanictis terlinguae new species	*Bryanictis* new species
Insectivora	Euarchonta
Mixodectidae	Mixodectidae
Mixodectes malaris	*Mixodectes malaris*
?Primates	Primates
Microsyopidae	"Palaechthonidae"
Palaechthon nacimienti	*Plesiolestes nacimienti*
"Condylarthra"	"Condylarthra"
Mioclaenidae	Mioclaenidae
Promioclaenus sp.	*Promioclaenus* cf. *P. lemuroides*
TMM locality 42327, "Dogie"	
Marsupialia	Metatheria
Didelphidae	Peradectidae
Peratherium sp.	*Peradectes* sp.
Cimolesta	Cimolesta
Palaeoryctidae	Cimolestidae
Gelastops sp.	Cimolestidae indeterminate
Carnivora	Carnivoramorpha
Didymictidae	Viverravidae
Bryanictis terlinguae new species	*Bryanictis* new species
"Condylarthra"	"Condylarthra"
Arctocyonidae	"Triisodontidae"
Eoconodon sp.	cf. *Goniacodon levisanus*
Periptychidae	Periptychidae
Carsioptychus coarctatus	*Periptychus carinidens*
Haploconus inopinatus	*Haploconus* sp.
Mioclaenidae	Mioclaenidae
Ellipsodon priscus	*Ellipsodon* cf. *E. inaequidens*
Nexus plexus new genus and species	*Mioclaenus* new species

bly heated the underlying deposits above the Curie temperature of titanohematite, causing these grains to be reset, which could also have resulted in the overprinted interval.

All reversed polarity samples in the section have a natural remanent magnetization (NRM) that overlaps with the modern direction, suggesting all samples have a modern overprint. In samples where titanohematite is the primary magnetic carrier, remanence is lost at low temperatures during the stepwise thermal demagnetization process. In most of these samples, low-temperature magnetometry curves also indicate a minor presence of magnetite, which could hold remanence beyond the Curie temperature of titanohematite. The demagnetization behavior of samples with titanohematite as the primary magnetic carrier behaved in two ways. The demagnetization behavior either (1) was too erratic for a statistically significant reversed direction to be calculated (Fig. 3F) or (2) was measurable to ~300 °C, such that a reversed direction could be calculated using a great circle (Fig. 3D). We interpret samples for which we were able to calculate a reversed direction to have had a larger proportion of magnetite than samples that behaved erratically. Given that we calculated several lines and great circles indicating a reversed direction within this interval, we interpret the entire interval to be reversed with a strong normal overprint (Fig. 2).

Relationship of Polarity Stratigraphy to GPTS

We correlated the local polarity stratigraphy to the GPTS using a combination of vertebrate paleontology, $\delta^{13}C$ values of carbonate nodules (Nordt et al., 2003), detrital sanidine ages, and stratigraphic thickness (Fig. 10). Using these methods, we correlated our polarity stratigraphy to the GPTS as follows: A+ to ≥C32n, B– to C31r, C+ to C31n, D–.1 to C29r, and D–.2 to C27r.

The B– and C+ intervals were correlated to C31r and C31n, respectively, based on the presence of dinosaur faunas and stratigraphic thickness. The change from reversed polarity to normal polarity in the section was pinned to the boundary between C31r and C31n (Ogg, 2012). Given that the strata are a series of stacked paleosols over this interval, there is assumed to be no significant amount of time missing. It is possible that the B– and C+ intervals could correlate to C30r and C30n; however, C30r only spans 173 k.y. (Ogg, 2012), and the B– interval corresponds to 77 m of section. Deposition over such a short time interval seems unlikely (see discussion of sedimentation rates in the following). The detrital age of 76.28 ± 0.06 Ma from SS02, near the base of the B– interval, suggests the sandstone bodies represent reworked older sediments.

Because the B– interval was correlated to C31r, the underlying A+ interval was correlated to C32n. However, there is only one stratigraphic locality associated with this interval and no fossils from Dawson Creek to constrain its age further. The mammalian fauna of the Aguja Formation correlated to the Judithian, which occurs from ca. 79 to 74 Ma (Cifelli et al., 2004), suggesting the Aguja interval is likely older than C32n. Additionally, geochronologic studies on the Aguja Formation in other areas of the park also have indicated that the age may be older (Befus et al., 2008; Breyer et al., 2007). Thus, correlation to C32n represents the minimum age for the Aguja Formation. The detrital age of 76.28 ± 0.06 Ma in the overlying B– interval also suggests that the A+ interval could be older.

We interpret the D–.1 interval to correlate to C29r for two reasons. First, the detrital sanidine ages support correlation to C29r. At the base of the D–.1 interval, the SS07 detrital age of 68.83 ± 0.13 Ma corresponds to C31n, and the SS08 detrital age of 68.08 ± 0.03 Ma, from the middle of the D–.1 interval, corresponds to C30n. Since the deposits in this interval are reversed, these detrital ages constrain the interval to either C29r or C30r. Second, the Cretaceous-Paleogene boundary, which occurs within C29r (Ogg, 2012), is within the D–.1 polarity interval (Lehman, 1990; Wiest et al., 2018), indicating D–.1 is correlative to C29r and not C30r.

There is a significant sandstone body with an erosive base indicating an unconformity between D–.1 and D–.2 (Fig. 2; Atchley et al., 2004). The occurrence of Torrejonian mammals, which first appear in C28n (Lofgren et al., 2004), above this sandstone means that the D–.2 interval cannot correlate to C29r. The identification of To2 mammals, which occur in C27r in the San Juan Basin (Lofgren et al., 2004; Williamson, 1996), allows us to correlate the D–.2 interval to C27r (Fig. 10). The maximum depositional age of sample SS13, located in the sandstone overlying P28, is defined by a single grain dated to 65.9 ± 0.4 Ma, which supports an early Paleocene age. Because we do not have any other age constraints for this interval, we assumed the base of the D–.2 interval starts at the base of C27r, but we note that this is a maximum age for this interval.

Sedimentation Rate Calculations

There are multiple chronostratigraphic tie points within the D–.1 local polarity interval, and therefore we used that interval to develop a sedimentation rate model for the Dawson Creek section. To determine the sedimentation rates for C29r, we first used the Cretaceous-Paleogene boundary (66.043 Ma; Renne et al.,

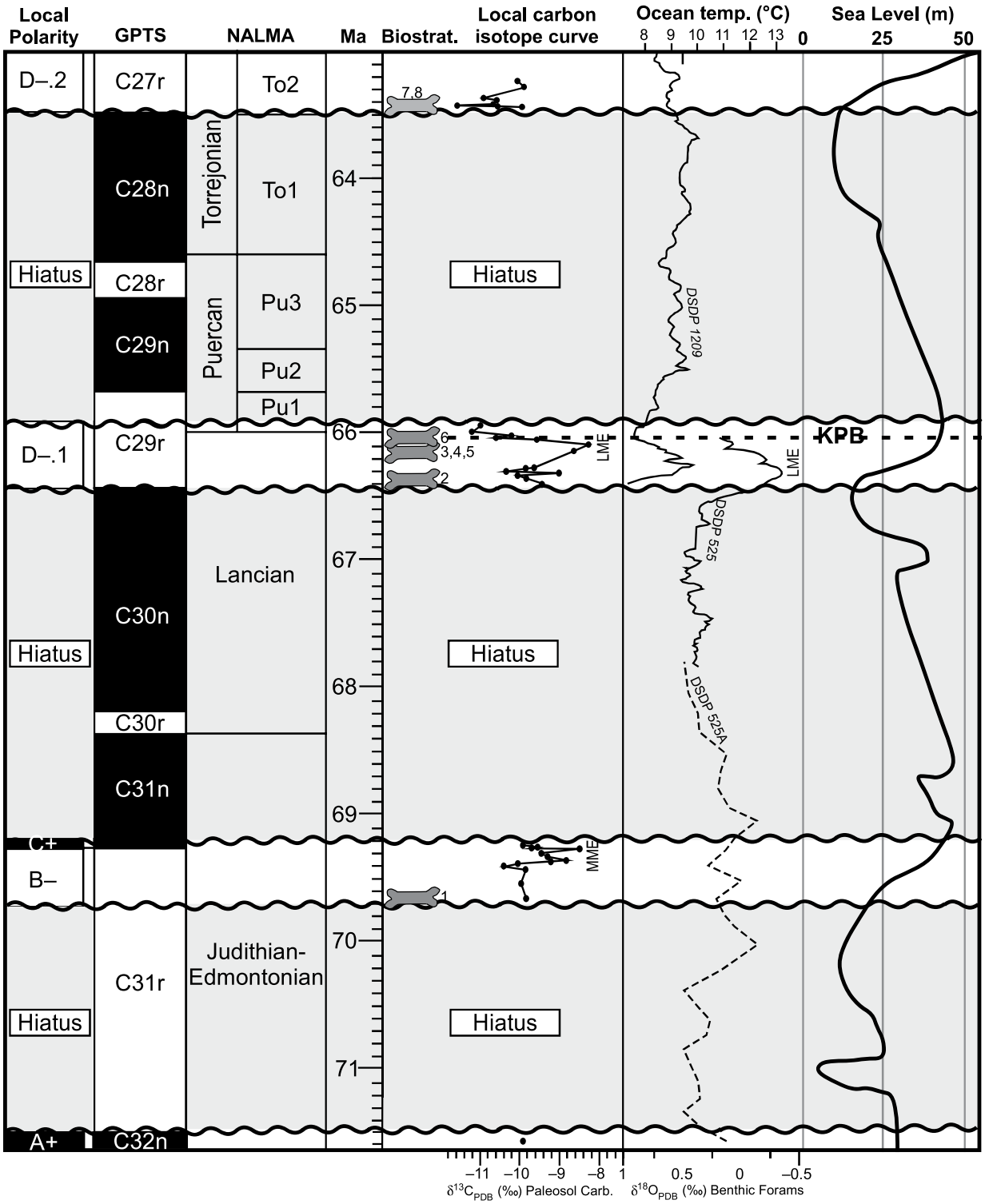

Figure 10. Summary chart for the Dawson Creek section showing correlations among local polarity stratigraphy, geomagnetic polarity time scale (GPTS; Ogg, 2012), North American Land Mammal Ages (NALMAs; Woodburne, 2004), time scale (Gradstein et al., 2012), and local fossil localities. Fossil localities: 1—LSU VL-110; 2—LSU VL-149; 3—TMM 41450, LSU VL-106; 4—LSU VL-112; 5—LSU VL-145; 6—TMM 41501; 7—TMM 41400, "Tom's Top" (LSU VL-111); 8—LSU VL-109 (Lehman, 1990). Gray boxes highlight hiatuses in the record. KPB—Cretaceous-Paleogene boundary; MME—mid-Maastrichtian event; LME—late Maastrichtian event. $\delta^{13}C_{PDB}$ isotopic values from pedogenic carbonate are modified from Nordt et al. (2003), where PDB—Peedee belemnite. $\delta^{18}O_{PDB}$ isotopic values from benthic foraminifera are from Deep Sea Drilling Project (DSDP) 1209 in the North Pacific (Westerhold et al., 2011), and DSDP 525A (Li and Keller, 1998a) and DSDP 525 (Li and Keller, 1998b) in the South Atlantic. Corresponding marine temperatures were calculated from stable O isotopes using equation from Erez and Luz (1983), assuming a –1.2‰ ice-free standard mean ocean water (SMOW). Global sea-level curve is from Miller et al. (2005).

2013), which occurs at 172 m in the section (Wiest et al., 2018), and the late Maastrichtian event, which occurs at 154 m in the section (Nordt et al., 2003) as known tie points. The late Maastrichtian event has been estimated to occur ~250 k.y. before the boundary (Li and Keller, 1998a, 1998b; Westerhold et al., 2011; Tobin et al., 2012), and so we used an age of 66.25 Ma (C29r) for it (Fig. 10). Using these tie points, the resulting sedimentation rate is 87 m/m.y. Extrapolation of this sedimentation rate throughout the underlying portion of the reversed D–.1 interval would put the base of the polarity zone at 66.77 Ma, which is well within C30n (Ogg, 2012). Given that this interval is of reversed polarity, the age estimate is impossible, and so we interpret the sedimentation rate of 87 m/m.y. to be too slow.

Second, we assumed the maximum depositional age for the base of the D–.1 interval to correlate to the base of C29r or 66.398 Ma (Ogg, 2012). A sedimentation rate was then calculated from the base of the D–.1 local polarity zone to the Cretaceous-Paleogene boundary at 172 m, resulting in a rate of 203 m/m.y. This sedimentation rate estimates an age of 66.157 Ma for the onset of the late Maastrichtian event, which is similar to age estimates from the marine record (Li and Keller, 1998a, 1998b; Westerhold et al., 2011; Tobin et al., 2012). Thus, we favor the second interpreted sedimentation rate, and we extrapolated it to the remainder of the section to estimate the durations of deposition (Fig. 10). The B– interval spans 379 k.y., the C+ interval spans 54 k.y., the D–.1 interval spans 459 k.y., and the D–.2 interval spans 280 k.y.

Unconformities

The magnetostratigraphy from B.J. MacFadden (*in* Standhardt, 1986) correlated the section to C30n to C28r with no recognized unconformities. Atchley et al. (2004) documented unconformities in the section, but they concluded that the unconformities did not span any significant amount of time. Our new age constraints indicate that the Dawson section spans from C32n to C27r (71.6 Ma to 63.2 Ma) with significant hiatuses (Fig. 10), which supports the suggestion in Nordt et al. (2003) that considerable time is missing from the section. The hiatuses in the section correspond with amalgamated sandstone channel complexes, suggesting incision into the landscape. Based on our chron assignments and sedimentation rate estimates, the minimum duration for the hiatuses between the A+ and B– intervals spans ~1.75 m.y., that between C+ and D–.1 spans ~2.82 m.y., and that between D–.1 and D–.2 spans ~2.4 m.y. Mammalian biostratigraphy from the Javelina and Black Peaks Formations supports the duration of the unconformity between D–.1 and D–.2, because the last occurrence of Lancian dinosaurs near the top of the Javelina Formation and the lowest occurrence of Torrejonian mammals suggest a hiatus of ~2.5 m.y. (66.04 Ma for the Cretaceous-Paleogene boundary to 64.49 for base of C27r; Ogg, 2012). The occurrence of Judithian mammals in the Aguja Formation (ca. 79–74 Ma; Cifelli et al., 2004) and the Lancian dinosaur assemblage of the Javelina Formation (ca. 69–66 Ma; Cifelli et al., 2004) suggest that the unconformity between the A+ and B– intervals is likely longer than ~1.75 m.y.

The relationship between the section and associated hiatuses and the global sea-level curve from Miller et al. (2005) in Figure 10 demonstrates that the hiatuses are associated with falling stage and lowstand tracts, while intervals of deposition occurred during transgressive and highstand tracts. Increases in accommodation due to relative sea-level rise could have resulted in deposition along the coastal plain, while relative sea-level fall resulted in loss of accommodation and nondeposition and/or erosion (e.g., Wright and Marriott, 1993; Shanley and McCabe, 1994). The detrital ages also suggest that the sediment deposited in the section represents recycled material from the missing time intervals. These results support the conclusion in Atchley et al. (2004), who argued that the deposition of the section was controlled by eustatic sea level—however, at a different time scale than previously suggested. The trend of deposition during transgressive and highstand system tracts and nondeposition/erosion during falling stage and lowstand tracts provides an independent check on the reasonability of the calculated sedimentation rate, as deposition throughout the section is internally consistent.

Biostratigraphic Implications

A Lancian biostratigraphic age for the middle and upper parts of the Javelina Formation (which also includes the base of the Black Peaks Formation of some workers; e.g., Lehman and Busbey, 2007; Cobb, 2016) is based on the presence of three dinosaurs: *Alamosaurus*, *Tyrannosaurus rex*, and *Torosaurus*, which have been regarded as part of its distinctive *Alamosaurus* fauna (Lehman, 2001; Lehman et al., 2006). *Alamosaurus sanjuanensis* has been reported from several latest Cretaceous faunas restricted to the American Southwest: the North Horn Formation of central Utah, the Naashoibito Member of the Kirtland Formation of the San Juan Basin of northwestern New Mexico, the McRae Formation of central New Mexico, and the Javelina Formation of west Texas. *Alamosaurus*, *Tyrannosaurus rex* or cf. *T. rex*, and the large ceratopsian *Torosaurus utahensis* or a similar taxon (identified as either *Torosaurus* cf. *T. utahensis* [Big Bend National Park] or *Ojoceratops*, a taxon considered by some workers to be synonymous with *Triceratops* [e.g., Longrich, 2011] or *To. utahensis* [see Wick and Lehman, 2013]) are present in all the faunas. None of these taxa is known from pre-Lancian-age faunas, and *Tyrannosaurus* is restricted to Lancian faunas of the northern Rocky Mountain region, supporting a Lancian assignment for the faunas of the Javelina Formation. Additionally, our age constraints indicate that the dinosaur fauna in the Javelina Formation is confined to C29r. Thus, it is contemporaneous with the dinosaur fauna of the Hell Creek Formation in the Northern Great Plains. The Hell Creek Formation dinosaur fauna is the most complete, continuous end-Cretaceous North American record and has been well studied with respect to dinosaur diversity prior to the boundary (e.g., Sheehan et al., 1991; Pearson et al., 2002; Fastovsky and Sheehan, 2005; Fastovsky and Bercovici, 2016). Our age constraints for the Dawson Creek section indicate that differences between the Javelina and Hell Creek faunas are not the result of the faunas being different ages, as suggested by Lucas et al. (2016). Instead, the differences in the faunas are likely driven by other factors, such as isolation between populations and/or environmental conditions, leading to endemism and provinciality in the latest Cretaceous as suggested by Lehman (1987, 2001). Additionally, it suggests that the magnitude of extinction at the Cretaceous-Paleogene boundary may have been larger than previously suggested (e.g., Brusatte et al., 2015), because these taxa, restricted to the American Southwest, also likely went extinct at the boundary. Future work comparing the Javelina and Hell Creek dinosaur faunas will be valuable for evaluation of dinosaur endemism, provinciality, and extinction.

The mammalian fauna in the Black Peaks Formation has been reassigned as age equivalent to Torrejonian 2 faunas found elsewhere in western North America. Any difference between the mammals found in Dawson Creek and other Torrejonian localities would reflect environmental or biogeographic variability rather than temporal differences. Thus, the Black Peaks fauna is an important addition with which to evaluate North American early Paleocene mammalian diversity and biostratigraphy across other basins.

Paleoclimate Implications

Our age constraints suggest that the two warming events presented in Nordt et al. (2003) document rapid (<200 k.y.) changes in climate

within the Maastrichtian. At the top of the B–interval, the pedogenic carbonate $\delta^{13}C$ values previously identified as the mid-Maastrichtian event occur (Nordt et al., 2003). The age constraints in this paper assign the mid-Maastrichtian event an age between 69.35 and 69.30 Ma. The mid-Maastrichtian event observed in the marine record contains multiple peaks in isotopic values, one of which occurs from ca. 69.0 to 69.4 Ma (Li and Keller, 1998a, 1998b), suggesting a possible correlation (Fig. 10). Using the sedimentation rate that was calculated independent of the marine record–late Maastrichtian event chemostratigraphic correlation, the onset of the late Maastrichtian event in paleosol 19 is at 66.157 Ma, with the peak excursion value occurring at 66.092 Ma. These ages are in general agreement with the marine record, where the peak excursion values occur at 66.25 Ma (Li and Keller, 1998a, 1998b; Westerhold et al., 2011). However, it should be noted that there was likely a sedimentation rate change associated with the late Maastrichtian event in the Dawson Creek section, as suggested by the much lower sedimentation rate calculated between the Cretaceous-Paleogene boundary and the onset of the late Maastrichtian event (87 m/m.y.) compared to the sedimentation rate calculated for the entire D–.1 interval from the Cretaceous-Paleogene boundary and the assumed base of C29r at the base of the D–.1 zone (203 m/m.y.). Thus, it is possible that the age estimated here for the late Maastrichtian event from the calculated sedimentation rate is too young. Nonetheless, the age estimate supports the correlation between the terrestrial late Maastrichtian greenhouse event (Nordt et al., 2003) and the greenhouse event recorded in the marine record (Li and Keller, 1998a, 1998b; Westerhold et al., 2011; Tobin et al., 2012).

Our age constraints demonstrate that the Dawson Creek section correlates differently to strata in Big Bend National Park and western North America than previously thought. The Dawson Creek C27r strata correlate with the lower portion of the west Tornillo Flat section in the northern area of Big Bend, where pedogenic carbonate carbon and oxygen isotopes have also been characterized through the Eocene (Bataille et al., 2016). Bataille et al. (2016) observed a correlation between early Paleogene global temperature trends and the sediment accumulation rates and lithostratigraphy, concluding climate was the dominant control on deposition rather than global sea level, as we suggest. However, the Tornillo Flats and Dawson Creek sections are not age equivalent. The Dawson Creek section is predominantly Cretaceous, while the Tornillo Flat section is predominately Paleogene, which suggests the primary controls on deposition in the Big Bend region changed from eustatic sea level in the Late Cretaceous and early Paleocene to climate in the middle Paleocene and Eocene, possibly reflecting the retreat of the Western Interior Seaway in the Paleogene (Davidoff and Yancey, 1993). The Dawson Creek C27r strata also correlate to terrestrial deposits of the San Juan Basin, New Mexico, where work is ongoing to reconstruct paleosol bulk carbon $\delta^{13}C$ values and climate trends from paleosol geochemical proxies (e.g., Secord et al., 2016; Leslie et al., 2016). The age model for Dawson Creek presented here constrains the timing of climate trends from the Late Cretaceous through early Paleocene, bolstering the significance of the Dawson Creek section as part of the North American terrestrial record.

CONCLUSIONS

Paleomagnetic analysis of the Dawson Creek section in Big Bend National Park, west Texas, combined with reexamination of the fauna, indicates the section correlates to C32n-C31n, C29r, and C27r of the GPTS, with three large hiatuses that are longer than 1.5 m.y. each. These hiatuses correspond to falling stage and lowstand tracts of the global sea-level curve, while deposition correlates to transgressive and highstand tracts (Miller et al., 2005), indicating that eustatic sea-level change was the primary driver of environments of deposition within the Dawson Creek section. Rock magnetic analyses indicate that the dominant magnetic carrier in the Aguja and Black Peaks Formations is titanomagnetite, while the Javelina Formation has varying magnetic carriers, including hematite, magnetite, and maghemite. We conclude that the overprint interval surrounding the Cretaceous-Paleogene boundary was likely a result of titanohematite that was reset by burial or overlying basaltic flows.

This new age model has implications for biostratigraphic and isotopic correlations between the Big Bend area and other Cretaceous–Paleogene basins across North America.

The Javelina Formation dinosaur fauna is limited to C29r, and it is age equivalent to the dinosaur fauna of the Hell Creek Formation in the Northern Great Plains, which supports the concept of provinciality. Additionally, it implies that the Cretaceous-Paleogene extinction of non-avian dinosaurs was larger than previously suggested, because all nonavian dinosaur taxa endemic to the Big Bend area also went extinct at the boundary. The mammalian fauna previously identified as Puercan by Standhardt (1986) is reidentified as Torrejonian and allows for future diversity comparisons to other basins. This is one of only a few Torrejonian faunas in North America, which makes it important for understanding mammalian evolution following the Cretaceous-Paleogene boundary on both local and regional scales. Last, our findings show that the mid-Maastrichtian and late Maastrichtian greenhouse events documented by Nordt et al. (2003) represent rapid (<200 k.y.) changes in climate during the end-Cretaceous and correlate closely with the marine record. This work contributes to ongoing work in developing a more complete Late Cretaceous through Paleogene chronology for southern North America through a combination of detrital sanidine dates, magnetostratigraphy, and biostratigraphy, and it suggests that the application of the method to other areas in Big Bend would significantly improve the chronology of this important region.

APPENDIX: THERIAN MAMMALS FROM THE LOWER BLACK PEAKS FORMATION

Vertebrate fossils are found within the Javelina and Black Peaks Formations in the Dawson Creek section (Fig. 10). Fossil mammals from two localities, TMM locality 41400 (LSU VL-111; Tom's Top in Dawson Creek), and TMM locality 42327 (LSU VL-108; Dogie), were originally described by Schiebout (1974). LSU VL-109 ("Hot White"; locality 8, Fig. 2) yielded turtle, lizard, and crocodilian fossils (Standhardt, 1986). Additional fossils were later collected by Standhardt (1986) using screen-washing methods and described in an unpublished dissertation (accessible via Louisiana State University Digital Commons: https://digitalcommons.lsu.edu/cgi/viewcontent.cgi?referer=https://www.google.com/&httpsredir=1&article=5208&context=gradschool_disstheses). The fauna has appeared primarily in faunal lists (Schiebout et al., 1987; Standhardt, 1995) and was briefly evaluated by Williamson (1996). The only mammal previously described in the published literature is a single specimen of a multituberculates mammal from Tom's Top, *Stygimys vastus*, described by Lofgren et al. (2005). *Stygimys* is known from the Puercan through the Torrejonian of western North America, and the species *S. vastus* is endemic to the Tom's Top locality and therefore does not aid in refining its biostratigraphic correlation. The therian mammals from these faunas are illustrated and briefly described here.

Standhardt (1986) reported the presence of *Eoconodon coryphaeus* from locality LSU VL-107 ("Glen Eleven"), a locality outside the study area, near Glen Draw, 3.4 km southeast of Glenn Springs. Standhardt (1986) was not able to precisely place this locality into any regional stratigraphic section, because it is within faulted sediments in a syncline. We included a reassessment of this specimen because it was identified as a mammal known elsewhere only from the Puercan.

Next, we present the systematic paleontology and a brief description of the reidentified material. A more complete description and discussions are available in the supplemental files (see footnote 1).

SYSTEMATIC PALEONTOLOGY

Infraclass METATHERIA Huxley, 1880
Family PERADECTIDAE Trouessart, 1879
Genus PERADECTES Matthew and Granger, 1921
Peradectes sp.
(Figs. 8A–8D)

Peratherium sp. Standhardt, 1986, p. 210, fig. 68.
Material—LSU V-895, right partial M?; and LSU V-705, left m? from TMM locality 42327.
Description—A small metatherian mammal represented by a partial upper molar (LSU V-895; Fig. 8A) and a lower molar (LSU V-705; Figs. 8B–8D).

Order CIMOLESTA McKenna, 1975
Family CIMOLESTIDAE Marsh, 1889
Genus and species indeterminate
(Figs. 8E–8G)
Gelastops sp. Standhardt, 1986, p. 213, fig. 69.
Material—LSU V-708, left P3; and LSU V-841, partial right M2 from TMM locality 42327.
Description—A small cimolestid represented by a complete crown of a poorly preserved and abraded left P3 (LSU V-708; Figs. 8E–8F) and a partial M2 (LSU V-841; Fig. 8G) that includes the mesial and lingual portion of the tooth, including part of the paracone and a complete parastylar lobe and the protocone and talon basin.

Legion CARNIVORAMORPHA Wyss and Flynn, 1993
Family VIVERRAVIDAE Wortman and Matthew, 1899
Genus BRYANICTIS MacIntyre, 1966
Bryanictis new species
(Fig. 8H–8L)
Protictis (Bryanictis) terlinguae Standhardt, 1986, p. 218, figs. 71, 72. [nomen nudum]
Material—TMM 41400–10, left p4 from TMM locality 41400, and LSU V-709, incomplete P3 from TMM locality 42327.
Description—A small viverravid carnivoramorph representing a new species of *Bryanictis*, represented by at least two isolated teeth, an incomplete P3 (LSU V-709; Figs. 8H–8I) and a p4 (TMM 41400–10; Figs. 8J–8L). Standhardt (1986) referred an additional specimen to this taxon, consisting of an isolated p2 (LSU V-960). However, this specimen could not be located for this study.

Order DERMOPTERA Illiger, 1811
Family MIXODECTIDAE Cope, 1883
Genus MIXODECTES Cope, 1883
Mixodectes malaris Cope, 1883
(Fig. 8M)
Indrodon malaris Cope, 1883, p. 60.
Mixodectes malaris Cope, 1883 [see Szalay, 1969 for synonymy]; Rigby, 1980, p. 63, Table 16; Taylor, 1984, p. 147, Table 10; Standhardt, 1986, p. 222, fig. 73; Williamson, 1996, p. 38.
Material—LSU V-924, partial left M3; and LSU V-928, partial left M2 from TMM locality 41400.
Description—Mixodectid *Mixodectes malaris*, represented by two fragmentary upper molars, a partial left M3 (LSU V-924; Fig. 8M) and a partial left M2 (LSU V-928). Unfortunately, the partial left M2 was not available for this study. The partial left M3 consists of the distal half of the crown.

Order PRIMATES Linnaeus, 1758
Family 'PALAECHTHONIDAE' Szalay, 1969
Genus PLESIOLESTES Jepsen, 1930
Plesiolestes nacimienti Wilson and Szalay, 1972
(Figs. 8N–8R)
Palaechthon nacimienti Wilson and Szalay, 1972, p. 5, figs. 2–9; Taylor, 1984, p. 164, Table 13; Standhardt, 1986, p. 225, fig. 74; Williamson and Lucas, 1993, p. 121; Williamson, 1996, p. 39.
Plesiolestes nacimienti (Wilson and Szalay, 1972). Gunnell, 1989, p. 24; Silcox and Williamson, 2012, p. 810, fig. 4.
Material—LSU V-921, right P4; TMM 41400-17, left M2; and LSU V-923, right m3 from TMM locality 41400.
Description—*Plesiolestes nacimienti*, represented by three isolated teeth, including a right P4 (LSU V-921; Fig. 8N), left M2 (LSU V-923; Fig. 8O), and right partial m3 (LSU V-923; Figs. 8P–8R).

Order 'CONDYLARTHRA' Cope, 1881b
Family PERIPTYCHIDAE Cope, 1882b
Genus HAPLOCONUS Cope, 1882a
Haploconus sp.
(Figs. 9A–9E)
Haploconus inopinatus Standhardt, 1986, p. 248, fig. 82.
Material—LSU V-710, partial right M1; LSU V-711, partial right M2; and LSU V-835, left m2 from TMM locality 42327.
Description—The periptychids "condylarth" *Haploconus*, represented by three partial teeth. Two isolated teeth represent a partial M1 (LSU V-710; Fig. 9A) and a partial M2 (LSU V-711; Fig. 9B) that likely come from a single individual.

Genus PERIPTYCHUS Cope, 1881a
Periptychus carinidens Cope, 1881a
(Figs. 9F–9H)
Periptychus carinidens Cope, 1881a, p. 337 [see Taylor, 1984 for synonymy]; Rigby, 1980, p. 111, pl. XIV, figs. 7–9, Table 42; Archibald, 1998, p. 312, fig. 20.3c; Williamson and Lucas, 1992, fig. 15i–k; Williamson and Lucas, 1993, p. 125; Williamson, 1996, p. 45.
Periptychus gilmorei Gazin, 1939, p. 272, fig. 3; Archibald, 1998, p. 313.
Carsioptychus coarctatus Standhardt, 1986, p. 243, fig. 81.
Material—LSU V-888, right m3; LSU V-873, right dentary fragment with partial m?; and LSU V-1554, right partial M? from TMM locality 42327.
Description—*Periptychus carinidens*, represented by a dentary fragment with a partial and highly abraded lower molar, an isolated partial right upper molar (LSU V-1554), and a nearly complete m3 (LSU V-888; Figs. 9F–9H).

Family MIOCLAENIDAE Osborn and Earle, 1895
Genus PROMIOCLAENUS Trouessart, 1904
Promioclaenus cf. *P. lemuroides* Matthew, 1897
(Figs. 9I–9J)
Promioclaenus sp. Standhardt, 1986, p. 256, fig. 84.
Ellipsodon priscus Standhardt, 1986 (in part), p. 251, fig. 83a.
Material—LSU V-875, right P3; and LSU V-920, partial left M3 from TMM locality 41400.
Description— *Promioclaenus* cf. *P. lemuroides*, represented by an isolated P3 (LSU V-875; Fig. 9I) and a partial M3 (LSU V-920; Fig. 9J).

Genus MIOCLAENUS Cope, 1881d
Mioclaenus new species.
(Figs. 9K–9U)
Nexus plexus Standhardt, 1986, p. 258, fig. 85. [nomen nudum]
Material—LSU V-890, left M2; LSU V-891, left M1; LSU V-833, left P4; LSU V-703, right partial dentary with erupting m2; LSU V-839, V-840, partial right m2; and LSU V-881, left m3 from TMM locality 42327.
Description—A small mioclaenid "condylarth," representing a new species of *Mioclaenus*, which represents the most complete taxon reported from TMM locality 42327. The new species is represented by an isolated, poorly preserved P4 (LSU V-833; Figs. 9K–9L), an isolated M1 (LSU V-891; Figs. 9M–9N), an isolated left M2 (LSU V-890; Figs. 9O–9P), an m2 (LSU V-703; Figs. 9Q–9R), a partial right m2 (LSU V-839, V840), and a left m3 (LSU V-881; Figs. 9S–9U).

Genus ELLIPSODON Scott, 1892
Ellipsodon cf. *E. inaequidens* Cope, 1884
(Figs. 9V–9Z)
Ellipsodon priscus Standhardt, 1986, p. 251 (in part), fig. 83B–H.
Material—LSU V-706, left M1; and LSU V-701, right m1 from TMM locality 42327.
Description—*Ellipsodon inaequidens*, represented by two teeth: a left M1 (LSU V-706; Figs. 9V–9W), and a right m1 (LSU V-701; Figs. 9X–9Z).

Family 'TRIISODONTIDAE' Scott, 1892
Genus GONIACODON Cope, 1888
cf. *Goniacodon levisanus* Cope, 1883
(Figs. 9AA–9BB)
Eoconodon sp. Standhardt, 1986, p. 238, fig. 84.
Material—LSU V-704, left M3 from TMM locality 42327.
Description—Cf. *Goniacodon levisanus*, represented by an isolated left M3 (LSU V-704; Figs. 9AA–9BB).

Genus TRIISODON Cope, 1881c
Triisodon quivirensis Cope, 1881c
(Fig. DR1; see text footnote 1)
Triisodon quivirensis Cope, 1881c, p. 485; Van Valen, 1978, p. 58; Williamson and Lucas, 1993, p. 123; Williamson, 1996, p. 41.
Triisodon antiquus Cope, 1882a, p. 193 [see Taylor, 1984 for synonymy]; Tomida, 1981, p. 230, pl. 10.2, figs. 1–2.
Eoconodon coryphaeus Standhardt, 1986, p. 232, fig. 77.
Material—LSU V-1156, partial right M2; and LSU V-1157, partial left m1 or m2 from LSU locality VL-107.
Description—Taxon *Triisodon quivirensis*, represented by fragments of two teeth (Fig. DR1 [see footnote 1]), portions of a dentary, and postcranial fragments. These were found in close association and likely represent a single individual. However, some of the individual fragments were given different specimen numbers.

ACKNOWLEDGMENTS

This work was conducted in Big Bend National Park on research permit BIBE-2014-SCI-005 to Leslie. This work was supported by the Society for Sedimentary Geology (SEPM), National Science Foundation grants EAR-132552, 0207750, and 1325544, the American Chemical Society Petroleum Research Fund (PRF#52822-DN18), Baylor University Department of Geosciences' Dixon Fund, and the Institute for Rock Magnetism. The Institute for Rock Magnetism is supported by the Instruments and Facilities program of the National Science Foundation, and by the University of Minnesota. We thank two anonymous reviewers for their helpful comments and B. Pratt and B. Singer for editorial assistance. Thanks go to A. Ramsey for assistance with sample collec-

tion and section measuring, L. Peters for assistance with sanidine separation, J. Schiebout and S. Ting of Louisiana State University (LSU) and M. Brown and C. Sagebiel of Texas Memorial Museum (TMM) for providing access and loan of fossil specimens, and J. Feinberg for helpful discussions.

REFERENCES CITED

Archibald, J.D., 1998, Archaic ungulates ("Condylarthra"), *in* Janis, C.M., Scott, K.M., and Jacobs, L.L., eds., Evolution of Tertiary Mammals of North America. Volume 1. Terrestrial Carnivores, Ungulates, and Ungulatelike Mammals: Cambridge, UK, Cambridge University Press, p. 292–331.

Atchley, S.C., Nordt, L.C., and Dworkin, S.I., 2004, Eustatic control on alluvial sequence stratigraphy: A possible example from the Cretaceous-Tertiary transition of the Tornillo Basin, Big Bend National Park, west Texas, USA: Journal of Sedimentary Research, v. 74, p. 391–404, https://doi.org/10.1306/102203740391.

Bataille, C.P., Watford, D., Ruegg, S., Lowe, A., and Bowen, G.J., 2016, Chemostratigraphic age model for the Tornillo Gorup: A possible link between fluvial stratigraphy and climate: Palaeogeography, Palaeoclimatology, Palaeoecology, v. 457, p. 277–289, https://doi.org/10.1016/j.palaeo.2016.06.023.

Befus, K.S., Hanson, R.E., Lehman, T.M., and Griffin, W.R., 2008, Cretaceous basaltic phreatomagmatic volcanism in west Texas: Maar complex at Pena Mountain, Big Bend National Park: Journal of Volcanology and Geothermal Research, v. 173, p. 245–264, https://doi.org/10.1016/j.jvolgeores.2008.01.021.

Breyer, J.A., Busbey, A.B., III, Hanson, R.E., Befus, K.E., Griffin, W.R., Hargrove, U.S., and Bergman, S.C., 2007, Evidence for Late Cretaceous volcanism in Trans-Pecos Texas: The Journal of Geology, v. 115, p. 243–251, https://doi.org/10.1086/510640.

Brochu, C.A., 2000, *Borealosuchus* (Crocodylia) from the Paleocene of Big Bend National Park, Texas: Journal of Paleontology, v. 74, p. 181–187, https://doi.org/10.1017/S0022336000031358.

Brusatte, S.L., Butler, R.J., Barrett, P.M., Carrano, M.T., Evans, D.C., Lloyd, G.T., Mannion, P.D., Norell, M.A., Peppe, D.J., Upchurch, P., and Williamson, T.E., 2015, The extinction of dinosaurs: Biological Reviews of the Cambridge Philosophical Society, v. 90, p. 628–642, https://doi.org/10.1111/brv.12128.

Carr, T.D., and Williamson, T.E., 2000, A review of Tyrannosauridae (Dinosauria, Coelurosauria) from New Mexico: New Mexico Museum of Natural History and Science Bulletin, v. 17, p. 113–146.

Carr, T.D., and Williamson, T.E., 2004, Diversity of late Maastrichtian Tyrannosauridae (Dinosauria: Theropoda) from western North America: Zoological Journal of the Linnean Society, v. 142, p. 479–523, https://doi.org/10.1111/j.1096-3642.2004.00130.x.

Cifelli, R.L., 1995, Therian mammals of the Terlingua Local Fauna (Judithian), Aguja Formation, Big Bend of the Rio Grande, Texas: Contributions to Geology, University of Wyoming, v. 30, p. 117–136.

Cifelli, R.L., Eberle, J.J., Lofgren, D.L., Lillegraven, J.A., and Clemens, W.A., 2004, Mammalian biochronology of the latest Cretaceous, *in* Woodburne, M.O., ed., Late Cretaceous and Cenozoic Mammals of North America: New York, Columbia University Press, p. 21–42, https://doi.org/10.7312/wood13040-004.

Clyde, W.C., Ramezani, J., Johnson, K.R., Bowring, S.A., and Jones, M.M., 2016, Direct high-precision U-Pb geochronology of the end-Cretaceous extinction and calibration of Paleocene astronomical timescales: Earth and Planetary Science Letters, v. 452, p. 272–280, https://doi.org/10.1016/j.epsl.2016.07.041.

Cobb, J., 2016, Sedimentology of the Cretaceous-Paleogene Boundary Interval in the Tornillo Group of West Texas [M.S. thesis]: Lubbock, Texas, Texas Tech University, 163 p.

Colbert, E.H., and Bird, R.T., 1954, A gigantic crocodile from the Upper Cretaceous beds of Texas: American Museum Novitates, v. 1688, p. 1–22.

Cope, E.D., 1881a, Mammalia of the lower Eocene beds: American Naturalist, v. 15, p. 337–338.

Cope, E.D., 1881b, On some Mammalia of the lowest Eocene beds of New Mexico: Proceedings of the American Philosophical Society, v. 19, p. 484–495.

Cope, E.D., 1881c, The temporary dentition of a new creodont: American Naturalist, v. 15, p. 667–669.

Cope, E.D., 1881d, Mammalia of the lowest Eocene: American Naturalist, v. 15, p. 829–831.

Cope, E.D., 1882a, Two new genera of the Puerco Eocene: American Naturalist, v. 16, p. 417–418.

Cope, E.D., 1882b, The Periptychidae: American Naturalist, v. 16, p. 832–833.

Cope, E.D., 1883, First addition to the fauna of the Puerco Eocene: Proceedings of the American Philosophical Society, v. 20, p. 545–563.

Cope, E.D., 1884, The Tertiary Marsupialia: American Naturalist, v. 18, no. 7, p. 686–697, https://doi.org/10.1086/273711.

Cope, E.D., 1888, Synopsis of the vertebrate fauna of the Puerco series: Transactions of the American Philosophical Society, v. 16, p. 298–361, https://doi.org/10.2307/1005393.

Davidoff, A.J., and Yancey, T.E., 1993, Eustatic cyclicity in the Paleocene and Eocene: Data from the Brazos River Valley, Texas: Tectonophysics, v. 222, p. 371–395, https://doi.org/10.1016/0040-1951(93)90360-V.

Davies, K.L., 1983, Hadrosaurian Dinosaurs of Big Bend National Park, Brewster County, Texas [M.S. thesis]: Austin, Texas, University of Texas, 235 p.

Dekkers, M.J., 1989, Magnetic properties of natural goethite: II. TRM behaviour during thermal and alternating field demagnetization and low-temperature treatment: Geophysical Journal International, v. 97, p. 341–355, https://doi.org/10.1111/j.1365-246X.1989.tb00505.x.

Dworkin, S., Nordt, L., and Atchley, S., 2005, Determining terrestrial paleotemperatures using the oxygen isotopic composition of pedogenic carbonate: Earth and Planetary Science Letters, v. 237, p. 56–68, https://doi.org/10.1016/j.epsl.2005.06.054.

Erez, J., and Luz, B., 1983, Experimental paleotemperature equation for planktonic foraminifera: Geochimica et Cosmochimica Acta, v. 47, p. 1025–1031, https://doi.org/10.1016/0016-7037(83)90232-6.

Fastovsky, D.E., and Bercovici, A., 2016, The Hell Creek Formation and its contribution to the Cretaceous-Paleogene extinction: A short primer: Cretaceous Research, v. 57, p. 368–390, https://doi.org/10.1016/j.cretres.2015.07.007.

Fastovsky, D.E., and Sheehan, P.M., 2005, The extinction of the dinosaurs in North America: GSA Today, v. 15, p. 4–10, https://doi.org/10.1130/1052-5173(2005)15<4:TEOTDI>2.0.CO;2.

Fisher, R.A., 1953, Dispersion of a sphere: Proceedings of the Royal Society of London, v. A217, p. 295–305, https://doi.org/10.1098/rspa.1953.0064.

Forster, C.A., Sereno, P.C., Evans, T.W., and Rowe, T.B., 1993, A complete skull of *Chasmosaurus mariscalensis* (Dinosauria: Ceratopsidae) from the Aguja Formation (late Campanian) of west Texas: Journal of Vertebrate Paleontology, v. 13, p. 161–170, https://doi.org/10.1080/02724634.1993.10011498.

France, D.E., and Oldfield, F., 2000, Identifying goethite and hematite from rock magnetic measurements of soils and sediments: Journal of Geophysical Research, v. 105, p. 2781–2795, https://doi.org/10.1029/1999JB900304.

Fronimos, J.A., and Lehman, T.M., 2014, New specimens of a titanosaur sauropod from the Maastrichtian of Big Bend National Park, Texas: Journal of Vertebrate Paleontology, v. 34, p. 883–899, https://doi.org/10.1080/02724634.2014.840308.

Gazin, C.L., 1939, A further contribution to the Dragon Paleocene fauna of central Utah: Journal of the Washington Academy of Sciences, v. 29, p. 273–286.

Gradstein, F.M., Ogg, J.G., Schmitz, M., and Ogg, G., 2012, The Geologic Time Scale 2012: Boston, Massachusetts, Elsevier, 1176 p.

Gunnell, G.F., 1989, Evolutionary History of Microsyopoidea (Mammalia? Primates) and the Relationship between Plesiadapiformes and Primates: University of Michigan Papers on Paleontology 27, 157 p.

Hunt, R.K., and Lehman, T.M., 2008, Attributes of the ceratopsian dinosaur *Torosaurus*, and new material from the Javelina Formation (Maastrichtian) of Texas: Journal of Paleontology, v. 82, p. 1127–1138, https://doi.org/10.1017/S0022336000055335.

Huxley, T.H., 1880, On the application of the laws of evolution to the arrangement of the Vertebrata and more particularly of the Mammalia: Proceedings of the Zoological Society of London, v. 43, p. 649–662.

Illiger, C., 1811, Prodromus systematis mammalium et avium additis terminis zoographicis utriusque classis: Berlin, C. Salfeld, 301 p., https://doi.org/10.5962/bhl.title.106965.

Jasinski, S.E., and Sullivan, R.M., 2011, Re-evaluation of Pachycephalosaurids from the Fruitland-Kirtland transition (Kirtlandian, late Campanian), San Juan Basin, New Mexico, with a description of a new species of *Stegoceras* and a reassessment of *Texacephale langstoni*: New Mexico Museum of Natural History and Science Bulletin, v. 53, p. 202–215.

Jepsen, G.L., 1930, New vertebrate fossils from the Lower Eocene of the Bighorn Basin, Wyoming: Proceedings of the American Philosophical Society, v. 69, no. 1, p. 117–131.

Kirschvink, J.L., 1980, The least-squares line and plane and the analysis of palaeomagnetic data: Geophysical Journal International, v. 62, p. 699–718, https://doi.org/10.1111/j.1365-246X.1980.tb02601.x.

Kuiper, K.F., Deino, A., Hilgren, F.J., Krijgsman, W., Renne, P.R., and Wijbrans, J.R., 2008, Synchronizing rock clocks of Earth history: Science, v. 320, p. 500–504, https://doi.org/10.1126/science.1154339.

Larson, D.W., and Currie, P.J., 2013, Multivariate analyses of small theropod dinosaur teeth and implications for paleoecological turnover through time: PLoS One, v. 8, p. e54329, https://doi.org/10.1371/journal.pone.0054329.

Lawson, D.A., 1972, Paleoecology of the Tornillo Formation, Big Bend National Park, Brewster County, Texas [M.S. thesis]: Austin, Texas, University of Texas at Austin, 182 p.

Lawson, D.A., 1975, Pterosaur from the latest Cretaceous of west Texas: Discovery of the largest flying creature: Science, v. 187, p. 947–948, https://doi.org/10.1126/science.187.4180.947.

Lawson, D.A., 1976, *Tyrannosaurus* and *Torosaurus*, Maestrichtian dinosaurs from Trans-Pecos, Texas: Journal of Paleontology, v. 50, p. 158–164.

Lehman, T.M., 1982, A Ceratopsian Bone Bed from the Aguja Formation (Upper Cretaceous), Big Bend National Park, Texas [M.S. thesis]: Austin, Texas, University of Texas, 209 p.

Lehman, T.M., 1985, Stratigraphy, Sedimentology, and Paleontology of Upper Cretaceous (Campanian-Maastrichtian) Sedimentary Rocks in Trans-Pecos, Texas [Ph.D. thesis]: Austin, Texas, University of Texas, 299 p.

Lehman, T.M., 1986, Late Cretaceous sedimentation in Trans-Pecos Texas, *in* Pause, P.H., and Spears, R.G., eds., Geology of the Big Bend Area and Solitario Dome, Texas: West Texas Geological Society Fieldtrip Guidebook 86-82, p. 105–110.

Lehman, T.M., 1987, Late Maastrichtian paleoenvironments and dinosaur biogeography in the western interior of North America: Palaeogeography, Palaeoclimatology, Palaeoecology, v. 60, p. 189–217, https://doi.org/10.1016/0031-0182(87)90032-0.

Lehman, T.M., 1989a, Upper Cretaceous (Maastrichtian) paleosols in Trans-Pecos Texas: Geological Society of America Bulletin, v. 101, p. 188–203, https://doi.org/10.1130/0016-7606(1989)101<0188:UCMPIT>2.3.CO;2.

Lehman, T.M., 1989b, *Chasmosaurus mariscalensis*, sp. nov., a new ceratopsian dinosaur from Texas: Journal of Vertebrate Paleontology, v. 9, p. 137–162, https://doi.org/10.1080/02724634.1989.10011749.

Lehman, T.M., 1990, Paleosols and the Cretaceous/Tertiary transition in the Big Bend region of Texas: Geology, v. 18, p. 362–364, https://doi.org/10.1130/0091-7613(1990)018<0362:PATCTT>2.3.CO;2.

Lehman, T.M., 1991, Sedimentation and tectonism in the Laramide Tornillo Basin of west Texas: Geology, v. 18, p. 363–364.

Lehman, T.M., 1997, Late Campanian dinosaur biogeography in the western interior of North America, *in* Wolberg, D., and Stump, E., eds., Dinofest International Proceedings: Philadelphia, Pennsylvania, The Academy of Natural Sciences, p. 223–240.

Lehman, T.M., 1998, A gigantic skull and skeleton of the horned dinosaur *Pentaceratops sternbergi* from New Mexico: Journal of Paleontology, v. 72, p. 894–906, https://doi.org/10.1017/S0022336000027220.

Lehman, T.M., 2001, Late Cretaceous dinosaur provinciality, *in* Tanke, D., and Carpenter, K., eds., Mesozoic Vertebrate Life: Bloomington and Indianapolis, Indiana University Press, p. 310–328.

Lehman, T.M., 2010, Pachycephalosauridae from the San Carlos and Aguja Formations (Upper Cretaceous) of west Texas, and observations of the frontoparietal dome: Journal of Vertebrate Paleontology, v. 30, p. 786–798, https://doi.org/10.1080/02724631003763532.

Lehman, T.M., and Barnes, K., 2010, Champsosaurus (Diapsida: Choristodera) from the Paleocene of west Texas: Paleoclimatic implication: Journal of Paleontology, v. 84, p. 341–345, https://doi.org/10.1666/09-111R.1.

Lehman, T.M., and Busbey, A.B., 2007, Big Bend Field Trip Guidebook: Society of Vertebrate Paleontology 67th Annual Meeting Field Trip Guidebook, 69 p.

Lehman, T.M., and Coulson, A.B., 2002, A juvenile specimen of the sauropod dinosaur *Alamosaurus sanjuanensis* from the Upper Cretaceous of Big Bend National Park, Texas: Journal of Paleontology, v. 76, p. 156–172, https://doi.org/10.1666/0022-3360(2002)076<0156:AJSOTS>2.0.CO;2.

Lehman, T.M., Mcdowell, F.W., and Connelly, J.N., 2006, First isotopic (U-Pb) age for the Late Cretaceous Alamosaurus vertebrate fauna of west Texas, and its significance as a link between two faunal provinces: Journal of Vertebrate Paleontology, v. 26, p. 922–928, https://doi.org/10.1671/0272-4634(2006)26[922:FIUAFT]2.0.CO;2.

Leslie, C.E., Secord, R., Peppe, D.J., Atchley, S., Williamson, T.E., Nordt, L.C., and Brusatte, S., 2016, Climatic and depositional history of the Lower Paleocene Upper Nacimiento Formation, San Juan Basin, New Mexico: Geological Society of America Abstracts with Programs, Abstract 287-7, v. 48, no. 7, https://doi.org/10.1130/abs/2016AM-287214.

Li, L., and Keller, G., 1998a, Maastrichtian climate, productivity and faunal turnovers in planktic foraminifera in South Atlantic DSDP sites 525 and 21: Marine Micropaleontology, v. 33, p. 55–86, https://doi.org/10.1016/S0377-8398(97)00027-3.

Li, L., and Keller, G., 1998b, Abrupt deep-sea warming at the end of the Cretaceous: Geology, v. 26, p. 995–998, https://doi.org/10.1130/0091-7613(1998)026<0995:ADSWAT>2.3.CO;2.

Linnaeus, C., 1758, Systema naturae per regna tria naturae, secundum classes, ordines, genera, species, cum characteribus, differentiis, synonymis, locis, v. 1: Regnum animale: Stockholm, Sweden, Laurentii Salvii, Editio decima, reformata, 823 p.

Lofgren, D.L., Lillegraven, J.A., Clemens, W.A., Gingerich, P.D., and Williamson, T.E., 2004, Paleocene biochronology: The Puercan through Clarkforkian land mammal ages, *in* Woodburne, M.O., ed., Late Cretaceous and Cenozoic Mammals of North America: Biostratigraphy and Geochronology: New York, Columbia University Press, p. 43–105, https://doi.org/10.7312/wood13040-005.

Lofgren, D.L., Scherer, B.E., Clark, C.K., and Standhardt, B., 2005, First record of *Stygimys* (Mammalia, Multituberculata, Eucosmodontidae) from the Paleocene (Puercan) part of the North Horn Formation, Utah, and a review of the genus: Journal of Mammalian Evolution, v. 12, p. 77–97, https://doi.org/10.1007/s10914-005-4865-9.

Longrich, N.R., 2011, *Titanoceratops ouranos*, a giant horned dinosaur from the late Campanian of New Mexico: Cretaceous Research, v. 32, p. 264–276, https://doi.org/10.1016/j.cretres.2010.12.007.

Longrich, N.R., Sankey, J., and Tanke, D., 2010, *Texacephale langstoni*, a new genus of pachycephalosaurid (Dinosauria: Ornithischia) from the Upper Campanian Aguja Formation, southern Texas, USA: Cretaceous Research, v. 31, p. 274–284, https://doi.org/10.1016/j.cretres.2009.12.002.

Longrich, N.R., Barnes, K., Clark, S., and Millar, L., 2013, Caenagnathidae from the Upper Campanian Aguja Formation of west Texas, a revision of the Caenagnathinae: Peabody Museum of Natural History Bulletin, v. 54, p. 23–49, https://doi.org/10.3374/014.054.0102.

Lucas, S.G., Sullivan, R.M., Lichtig, A.J., Dalman, S.G., and Jasinski, S.E., 2016, Late Cretaceous dinosaur biogeography and endemism in the Western Interior Basin, North America: A critical re-evaluation: New Mexico Museum of Natural History and Science Bulletin, v. 71, p. 195–213.

MacIntyre, G.T., 1966, The Miacidae (Mammalia, Carnivora): Part 1. The systematics of *Ictidopappus* and *Protictis*: Bulletin of the American Museum of Natural History, v. 131, p. 115–210.

Mannion, P.D., and Upchurch, G.R., Jr., 2011, A re-evaluation of the 'mid-Cretaceous sauropod hiatus' and the impact of uneven sampling of the fossil record on patterns of regional dinosaur extinction: Palaeogeography, Palaeoclimatology, Palaeoecology, v. 299, p. 529–540, https://doi.org/10.1016/j.palaeo.2010.12.003.

Marsh, O.C., 1889, Discovery of Cretaceous Mammalia: American Journal of Science, v. 38, no. 223, p. 81–92, https://doi.org/10.2475/ajs.s3-38.223.81.

Matthew, W.D., 1897, A revision of the Puercan fauna: Bulletin of the American Museum of Natural History, v. 9, p. 259–323.

Matthew, W.D., and Granger, W., 1921, New genera of Paleocene mammals: American Museum Novitates, v. 13, no. 7, p. 1–7.

McKenna, M.C., 1975, Toward a phylogenetic classification of the Mammalia, *in* Luckett, W.P., and Szalay, F.S., eds., Phylogeny of the Primates: New York, Plenum Press, p. 21–46, https://doi.org/10.1007/978-1-4684-2166-8_2.

Miller, K.G., Kominz, M.A., Browning, J.V., Wright, J.D., Mountain, G.S., Katz, M.E., Sugarman, P.J., Cramer, B.S., Christie-Blick, N., and Pekar, S.F., 2005, The Phanerozoic record of global sea-level change: Science, v. 310, p. 1293–1298, https://doi.org/10.1126/science.1116412.

Min, K., Mundil, R., Renne, P.R., and Ludwig, K.R., 2000, A test for systematic errors in $^{40}Ar/^{39}Ar$ geochronology through comparison with U/Pb analysis of a 1.1-Ga rhyolite: Geochimica et Cosmochimica Acta, v. 64, p. 73–98, https://doi.org/10.1016/S0016-7037(99)00204-5.

Nordt, L., Atchley, S., and Dworkin, S., 2003, Terrestrial evidence for two greenhouse events in the latest Cretaceous: GSA Today, v. 13, no. 12, p. 4–9, https://doi.org/10.1130/1052-5173(2003)013<4:TEFTGE>2.0.CO;2.

Nydam, R., Cifelli, R.I., and Rowe, T.B., 2013, Lizards and snakes of the Terlingua local fauna (late Campanian), Aguja Formation, Texas, with comments on the distribution of paracontemporaneous squamates throughout the western interior of North America: Journal of Vertebrate Paleontology, v. 33, p. 1081–1099, https://doi.org/10.1080/02724634.2013.760467.

Ogg, J.G., 2012, Geomagnetic polarity time scale, *in* Gradstein, F.M., Ogg, J.G., Schmitz, M.D., and Ogg, G.D., eds., The Geologic Time Scale: Oxford, UK, Elsevier, p. 85–113, https://doi.org/10.1016/B978-0-444-59425-9.00005-6.

Osborn, H.F., and Earle, C., 1895, Fossil mammals of the Puerco beds. Collection of 1892: Bulletin of the American Museum of Natural History, v. 7, p. 1–70.

Pearson, D.A., Schaefer, T., Johnson, K.R., Nichols, D.J., and Hunter, J.P., 2002, Vertebrate biostratigraphy of the Hell Creek Formation in southwestern North Dakota and northwestern South Dakota, *in* Hartman, J.H., Johnson, K.R., and Nichols, D.J., eds., The Hell Creek Formation and the Cretaceous-Tertiary Boundary in the Northern Great Plains: An Integrated Continental Record of the End of the Cretaceous: Geological Society of America Special Paper 361, p. 145–167.

Peppe, D.J., Evans, D.A.D., and Smirnov, A.V., 2009, Magnetostratigraphy of the Ludlow Member of the Fort Union Formation (Lower Paleocene) in the Williston Basin, North Dakota: Geological Society of America Bulletin, v. 121, p. 65–79.

Prieto-Márquez, A., 2014, Skeletal morphology of *Kritosaurus navajovius* (Dinosauria: Hadrosauridae) from the Late Cretaceous of the North American south-west, with an evaluation of the phylogenetic systematics and biogeography of Kritosaurini: Journal of Systematic Palaeontology, v. 12, p. 133–175, https://doi.org/10.1080/14772019.2013.770417.

Renne, P.R., Deino, A.L., Hilgen, F.J., Kuiper, K.F., Mark, D.F., and Mitchell, W.S., III, 2013, Time scales of critical events around the Cretaceous-Paleogene boundary: Science, v. 339, p. 684–687, https://doi.org/10.1126/science.1230492.

Rigby, J.K., 1980, Swain Quarry of the Fort Union Formation, Middle Paleocene (Torrejonian), Carbon County, Wyoming: Geologic Setting and Mammalian Fauna: Chicago, Illinois, University of Chicago, Evolutionary Monographs, 179 p.

Rivera-Sylva, H.E., Hedrick, B.P., and Dodson, P., 2016, A Centrosaurine (Dinosauria: Ceratopsia) from the Aguja Formation (late Campanian) of Coahuila, Mexico: PLoS One, v. 11, p. e0150529, https://doi.org/10.1371/journal.pone.0150529.

Rowe, T., Cifelli, R.L., Lehman, T.M., and Weil, A., 1992, The Campanian Terlingua local fauna, with a summary of other vertebrates from the Aguja Formation, Trans-Pecos Texas: Journal of Vertebrate Paleontology, v. 12, p. 472–493, https://doi.org/10.1080/02724634.1992.10011475.

Sampson, S.D., Loewen, M.A., Farke, A.A., Roberts, E.M., Forster, C.A., Smith, J.A., and Titus, A.L., 2010, New horned dinosaurs from Utah provide evidence for intracontinental dinosaur endemism: PLoS One, v. 5, p. e12292, https://doi.org/10.1371/journal.pone.0012292.

Sankey, J.T., 1998, Vertebrate Paleontology and Magnetostratigraphy of the Upper Aguja Formation (Late Campanian), Talley Mountain Area, Big Bend National Park [Ph.D. thesis]: Baton Rouge, Louisiana, Louisiana State University, 251 p.

Sankey, J.T., 2001, Late Campanian southern dinosaurs, Aguja Formation, Big Bend, Texas: Journal of Paleontology, v. 75, p. 208–215, https://doi.org/10.1017/S0022336000031991.

Sankey, J.T., 2008, Vertebrate paleoecology from microsites, Talley Mountain, Upper Aguja Formation (Late Cretaceous), Big Bend National Park, Texas, USA, *in* Sankey, J.T., and Baszio, S., eds., Vertebrate Microfossil Assemblages: Their Role in Paleoecology and Paleobiogeography: Bloomington, Indiana, Indiana University Press, p. 61–77.

Sankey, J.T., Standhardt, B.R., and Schiebout, J.A., 2005, Theropod teeth from the Upper Cretaceous (Campanian-Maastrichtian), Big Bend National Park, Texas, *in* Carpenter, K., ed., The Carnivorous Dinosaurs: Bloomington, Indiana, Indiana University Press, p. 127–152.

Schiebout, J.A., 1974, Vertebrate Paleontology and Paleoecology of Paleocene Black Peaks Formation, Big Bend National Park, Texas: Texas Memorial Museum Bulletin 24, 88 p.

Schiebout, J.A., Rigsby, C.A., Rapp, J.D., Hartnell, J.A., and Standhardt, B.R., 1987, Stratigraphy of Late Cretaceous, Paleocene, and early Eocene rocks of Big Bend National Park, Texas: The Journal of Geology, v. 95, p. 359–375, https://doi.org/10.1086/629135.

Scott, W.B., 1892, A revision of the North American Creodonta: Proceedings of the Academy of Natural Sciences of Philadelphia, v. 44, p. 291–323.

Secord, R., Leslie, C.E., Williamson, T.E., Peppe, D.J., and Brusatte, S., 2016, First recognition of climate hyperthermals in the Lower Paleocene record of the San Juan Basin, New Mexico, USA: Geological Society of America Abstracts with Programs, Abstract 311-11, v. 48, no. 7, https://doi.org/10.1130/abs/2016AM-278979.

Shanley, K.W., and McCabe, P.J., 1994, Perspectives on the sequence stratigraphy of continental strata: American Association of Petroleum Geologists Bulletin, v. 78, p. 544–586.

Sheehan, P.M., Fastovsky, D.E., Hoffmann, R.G., Berghaus, C.B., and Gabriel, D.L., 1991, Sudden extinction of the dinosaurs: Family-level patterns of ecological diversity during the latest Cretaceous, upper Great Plains,

U.S.A.: Science, v. 254, p. 835–839, https://doi.org/10.1126/science.11536489.

Silcox, M.T., and Williamson, T.E., 2012, New discoveries of early Paleocene (Torrejonian) primates from the Nacimiento Formation, San Juan Basin, New Mexico: Journal of Human Evolution, v. 63, no. 6, p. 805–833, https://doi.org/10.1016/j.jhevol.2012.09.002.

Sloan, R.E., 1969, Cretaceous and Paleocene terrestrial communities of western North America, *in* Yochelson, E.L., ed., Proceedings of the North American Paleontological Convention: Lawrence, Kansas, Allen Press, p. 427–453.

Sprain, C.J., Feinberg, J.M., Renne, P.R., and Jackson, M., 2016, Importance of titanohematite in detrital remanent magnetizations of strata spanning the Cretaceous-Paleogene boundary, Hell Creek region, Montana: Geochemistry Geophysics Geosystems, v. 17, p. 660–678, https://doi.org/10.1002/2015GC006191.

Standhardt, B.R., 1986, Vertebrate Paleontology of the Cretaceous/Tertiary Transition of Big Bend National Park, Texas [Ph.D. thesis]: Baton Rouge, Louisiana, Louisiana State University, 298 p.

Standhardt, B.R., 1995, Early Paleocene (Puercan) vertebrates of the Dogie locality, Big Bend National Park, Texas, *in* Santucci, V., and McClelland, L., eds., National Park Services Paleontological Research: Denver, Colorado, Natural Resources Publication Office, p. 46–48.

Sullivan, R.M., Boere, A.C., and Lucas, S.G., 2005, Redescription of the ceratopsid dinosaur *Torosaurus utahensis* (Gilmore, 1946) and a revision of the genus: Journal of Paleontology, v. 79, p. 564–582, https://doi.org/10.1666/0022-3360(2005)079<0564:ROTCDT>2.0.CO;2.

Szalay, F.S., 1969, Mixodectidae, Microsyopidae, and the insectivore-primate transition: Bulletin of the American Museum of Natural History, v. 140, p. 195.

Taylor, L.H., 1984, Review of Torrejonian Mammals from the San Juan Basin, New Mexico [Ph.D. thesis]: Tucson, Arizona, University of Arizona, 553 p.

Tobin, T.S., Ward, P.D., Steig, E.J., Olivero, E.B., Hilburn, I.A., Mitchell, R.N., Diamond, M.R., Raub, T.D., and Kirschvink, J.L., 2012, Extinction patterns, $\delta^{18}O$ trends, and magnetostratigraphy from a southern high-latitude Cretaceous–Paleogene section: Links with Deccan volcanism: Palaeogeography, Palaeoclimatology, Palaeoecology, v. 350–352, p. 180–188, https://doi.org/10.1016/j.palaeo.2012.06.029.

Tomida, Y., 1981, "Dragonian" fossils from the San Juan Basin and the status of the "Dragonian" land mammal "age," *in* Lucas, S.G., Rigby, J.K., Jr., and Kues, B.S., eds., Advances in San Juan Basin Paleontology: Albuquerque, New Mexico, University of New Mexico Press, p. 222–241.

Tomlinson, S.L., 1997, Late Cretaceous and Early Tertiary Turtles from the Big Bend Region, Brewster County, Texas [Ph.D. thesis]: Lubbock, Texas, Texas Tech University, 195 p.

Torsvik, T.H., Müller, R.D., Van der Voo, R., Steinberger, B., and Gaina, C., 2008, Global plate motion frames: Toward a unified model: Reviews of Geophysics, v. 46, p. RG3004, https://doi.org/10.1029/2007RG000227.

Trouessart, E.L., 1879, Catalogue des mammifères vivants et fossils: Insectivores: Revue et Magasin de Zoologie Pure et Appliquée, v. 3, no. 7, p. 219–285.

Trouessart, E.L., 1904, Catalogus Mammalium: Quinquenale Suplementum: Berlin, Friedlander, 929 p.

Tykoski, R.S., and Fiorillo, A.R., 2016, An articulated cervical series of *Alamosaurus sanjuanensis* Gilmore, 1922 (Dinosauria, Sauropoda) from Texas: New perspective on the relationship of North America's last giant sauropod: Journal of Systematic Paleontology, v. 15, o. 5, p. 339–364, https://doi.org/10.1080/14772019.2016.1183150. 27 p.

Van Valen, L., 1978, The beginning of the age of mammals: Evolutionary Theory, v. 4, no. 2, p. 46–80.

Wagner, J., 2001, The Hadrosaurian Dinosaurs (Ornithischia: Hadrosauridae) of Big Bend National Park, Brewster County [M.S. thesis]: Lubbock, Texas, Texas Tech University, 417 p.

Wagner, J.R., and Lehman, T.M., 2009, An enigmatic new lambeosaurine hadrosaur (Reptilia: Dinosauria) from the Upper Shale Member of the Campanian Aguja Formation of Trans-Pecos Texas: Journal of Vertebrate Paleontology, v. 29, p. 605–611, https://doi.org/10.1671/039.029.0208.

Watson, G.S., 1956, Analysis of dispersion on a sphere: Monthly Notices of the Royal Astronomical Society, v. 7, p. 153–159, https://doi.org/10.1111/j.1365-246X.1956.tb05560.x.

Weil, A., 1992, The Terlingua Local Fauna: Stratigraphy, Paleontology, and Multituberculate Systematics [M.S. thesis]: Austin, Texas, University of Texas at Austin, 119 p.

Westerhold, T., Röhl, U., Donner, B., McCarren, H.K., and Zachos, J.C., 2011, A complete high-resolution Paleocene benthic stable isotope record for the central Pacific (ODP Site 1209): Paleoceanography, v. 26, p. 1–13, https://doi.org/10.1029/2010PA002092.

Wick, S.L., 2014, New evidence for the possible occurrence of *Tyrannosaurus* in west Texas, and discussion of Maastrichtian tyrannosaurid dinosaurs from Big Bend National Park: Cretaceous Research, v. 50, p. 52–58, https://doi.org/10.1016/j.cretres.2014.03.010.

Wick, S.L., and Lehman, T., 2013, A new ceratopsian dinosaur from the Javelina Formation (Maastrichtian) of west Texas and implications for chasmosaurine phylogeny: Naturwissenschaften, v. 100, p. 667–682, https://doi.org/10.1007/s00114-013-1063-0.

Wick, S.L., Lehman, T.M., and Brink, A.A., 2015, A theropod tooth assemblage from the lower Aguja Formation (early Campanian) of west Texas, and the roles of small theropod and varanoid lizard mesopredators in a tropical predator guild: Palaeogeography, Palaeoclimatology, Palaeoecology, v. 418, p. 229–244, https://doi.org/10.1016/j.palaeo.2014.11.018.

Wiest, L.A., Lukens, W.E., Peppe, D.J., Driese, S.G., Tubbs, J., 2018, Terrestrial evidence for the Lilluput effect across the Cretacoues-Paleogene (K-Pg) boundary: Palaeogeography, Palaeoclimatology, Palaeoecology, v. 491, p. 161–169, https://doi.org/10.1016/j.palaeo.2017.12.005.

Williamson, T.E., 1996, The beginning of the age of mammals in the San Juan Basin, New Mexico; biostratigraphy and evolution of Paleocene mammals of the Nacimiento Formation: New Mexico Museum of Natural History and Science Bulletin, v. 8, p. 1–141.

Williamson, T.E., and Lucas, S.G., 1993, Stratigraphy and mammalian biostratigraphy of the Paleocene Nacimiento Formation, southern San Juan Basin, New Mexico: New Mexico Museum of Natural History and Science Bulletin, v. 43, p. 265–296.

Wilson, R.W., and Szalay, F.S., 1972, New paromomyid primate from the middle Paleocene beds, Kutz Canyon area, San Juan Basin, New Mexico: American Museum Novitates, v. 2499, p. 1–18.

Woodburne, M.O., ed., 2004, Late Cretaceous and Cenozoic Mammals of North America: Biostratigraphy and Geochronology: New York, Columbia University Press, 376 p., https://doi.org/10.7312/wood13040.

Wortman, J.L., and Matthew, W.D., 1899, The ancestry of certain members of the Canidae, the Viverradae, and Procyonidae: Bulletin of the American Museum of Natural History, v. 12, p. 109–138.

Wright, V.P., and Marriott, S.B., 1993, The sequence stratigraphy of fluvial depositional systems: The role of floodplain sediment storage: Sedimentary Geology, v. 86, p. 203–210, https://doi.org/10.1016/0037-0738(93)90022-W.

Wyss, A.R., and Flynn, J.J., 1993, A phylogenetic analysis and definition of the Carnivora, *in* Szalay, F.S., Novacek, M.J., and McKenna, M.C., eds., Mammal Phylogeny: Volume 2. Placentals: New York, Springer, p. 32–52, https://doi.org/10.1007/978-1-4613-9246-0_4.

Science Editor: Bradley S. Singer
Associate Editor: Brian R. Pratt

Manuscript Received 1 March 2017
Revised Manuscript Received 28 November 2017
Manuscript Accepted 29 December 2017

Printed in the USA